DEGREE PROJECT

Simulation of Frictional Melting at the Ski-Snow Interface

A Numerical Investigation of Surface Interactions, Frictional Heating, and Phase Change Mechanisms

Erik Jangenmalm

Engineering Physics and Electrical Engineering, master's level
2025

Luleå University of Technology
Department of Engineering Science and Mathematics

LULEÅ UNIVERSITY OF TECHNOLOGY

[This page intentionally left blank]

Preface

This thesis was written as part of the Master's programme in Engineering Physics and Electrical Engineering at Luleå University of Technology. The project was carried out during the spring of 2025 and focuses on simulating frictional melting at the ski–snow interface.

The past five months have been the most challenging, yet also the most rewarding, period of my academic journey. Having had the opportunity to explore my own curiosity, without the constraints of a rigid curriculum, has been both liberating and intellectually fulfilling. I can proudly say that I have given this project my all.

I would like to express my sincere gratitude to my supervisor, Andreas Almqvist, for his continuous support, insightful feedback, and encouragement throughout the project. I would also like to thank Roland Larsson for valuable discussions and expert input.

Special thanks go to all my friends and family for their encouragement and unwavering support throughout this period. Last but not least, I would like to thank the friends with whom I have shared an office over the past five months. You have made the process that much more enjoyable.

Luleå, June 2025

Erik Jangenmalm

Disclaimer

In this thesis project, AI tools have been utilised to support several stages of the work. Different search engines and suggestions from ChatGPT's deep research function have been used to retrieve relevant literature and references. ChatGPT and other AI-based assistants have contributed to improving the readability, structure, and clarity of written text by suggesting formulations and improving consistency. Additionally, AI has been employed to assist in code development, including generating boilerplate code, debugging, and exploring alternative solutions to simulation problems.

AI tools have also been used as a means to question and deepen the understanding of underlying concepts and methods, as well as to suggest complementary perspectives during the development of the work.

I acknowledge and understand that AI-generated content may contain hallucinations, biases, or inaccuracies. Therefore, all results, formulations, and conclusions presented in this thesis have been critically reviewed, validated, and referenced to ensure scientific correctness and integrity.

Abstract

This work presents a numerical investigation into the mechanisms of frictional melting at the ski–snow interface, with the aim of understanding the conditions under which localised meltwater films form during gliding. Using a combination of boundary element contact mechanics and an enthalpy-based heat conduction model, the study explores how surface roughness, snow temperature, ski base texture, and sliding speed influence frictional heat dissipation and phase change. Simulation results reveal critical thresholds for meltwater generation, highlighting the strong influence of contact pressure, duration, and material properties. The findings contribute to the broader understanding of snow tribology and have potential applications in ski base design and preparation strategies for optimising glide performance in winter sports.

Contents

1 Introduction

Performance in cross-country skiing is strongly influenced by friction between the ski–base and the snow surface. Glide performance not only affects skier energy efficiency but also has a major impact on competitive outcomes. Ski–snow tribology involves complex interactions, influenced by factors such as snow temperature, ski base texture, and snow grain morphology. The commonly observed low friction during gliding is attributed to the formation of a thin meltwater layer at the ski–snow interface [1].

Understanding the microscale physics of the ski–snow interaction is key to improving glide performance. Insights at this level can inform ski preparation, material design, and waxing strategies tailored for different snow conditions. This work aims to deepen our understanding of how frictional energy input leads to phase transitions at the snow interface. In the long term, this knowledge may support data-driven approaches to improving glide and gaining a competitive edge. The modelling techniques developed here could also be relevant to other scenarios involving dynamic contact with snow or ice.

The following section outlines previous research, problem formulation, specific objectives of this work, and the scope of the study.

1.1 Previous Research

The origin of the self-lubrication theory due to frictional heating dates back to 1939 with the work done by Bowden and Hughes [1]. Previously, self-lubrication due to pressure melting had been postulated. However, Bowden argued that it was improbable, as the pressure required to melt snow at $-20\,^{\circ}\mathrm{C}$ required a real contact area of 0.001 %.

If the ski is a good thermal conductor, the heat generated by friction is quickly conducted away from the contact zone. As a result, less heat remains available to induce surface melting, which in turn leads to a higher friction coefficient. This effect was demonstrated in experiments comparing a hollow ski made of ebony, a material with low thermal conductivity, to the same hollow body filled with mercury, which has a much higher thermal conductivity. The friction coefficient for the ebony ski was found to be reduced by a factor of 1.3–1.7 relative to the mercury-filled version. This provides strong evidence that frictional heating contributes significantly to the formation of the lubricating water film. By measuring the electrical conductivity between the sliding surfaces, the researchers estimated the film thickness to be approximately 70 µm [1]. This is about the same order of magnitude as the results of Ambach and Mayr [2] who used a capacitive probe to measure the thicknesses of the water film to 4–20 µm.

The work of Hasler et al. [3] sought to verify the existence of a water film under cross-country skis. A snow tribometer and an IR camera were used to calculate the temperature behind the skis for 5–25 $\mathrm{m\,s^{-1}}$ at a load of 428 N, which was deemed realistic conditions for skiing. The tribometer used had a tested accuracy of 2.2 % [4]. The contact spot temperature was calculated with

$$T_{\mathrm{cs}} = \frac{T_{\mathrm{av}} - T_{\mathrm{uncontacted}}(1 - A_{\mathrm{c}})}{A_{\mathrm{c}}} \tag{1}$$

where T_{cs} is contact spot temperature, T_{av} is the average pixel temperature, $T_{\mathrm{uncontacted}}$ is the temperature before contact, and A_{c} is the contact area. This leads to a strong dependence on the contact area A_{c}, see Fig. 1.

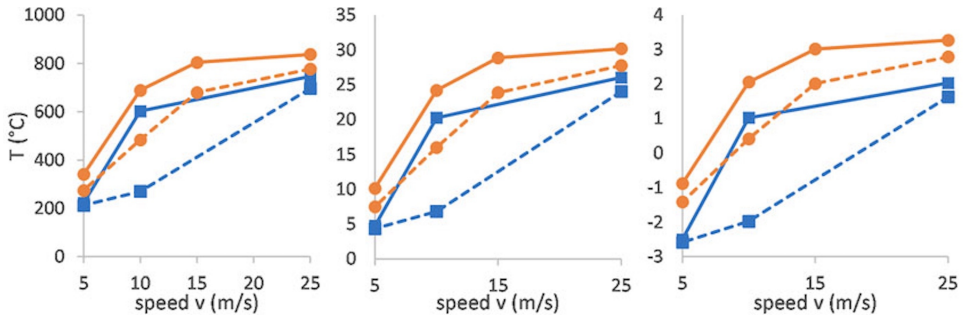

Figure 1: Contact spot temperatures of a flat ski (blue squares) and an XC ski (orange circles) vs. speed in the first run (dashed lines) and last run (solid lines) of five runs. Left: $A_r = 0.4\,\%$, Middle: $A_r = 10\,\%$, Right: $A_r = 50\,\%$. Adapted from Hasler et al. [3]

With the assumption that the contact spot temperature did not exceed 0 °C, a relative contact area of 21–98 % was estimated. By comparing the frictional heat generated to the heat flowing through the surfaces, Hasler argued that there had to be additional heat dissipation mechanisms in addition to conduction, concluding that the energy is most likely used for phase transformation. Earlier work by Hasler [5] showed an increase in temperature along the length of a cross-country ski during sliding. The highest temperature was measured behind the heel of the skier, followed by a decrease in temperature at the end of the ski. This is expected, in part because the pressure distribution of the ski–snow contact has its highest peak at that point (∼80 % of the total load) [5, 6, 7]. But also because snow/ice asperities that have been in contact with the ski longer will generate more heat, thereby also creating more meltwater [8]. Experiments by Siddiqui et al [9] seem to confirm the meltwater theory in the ski–snow interaction. They used humidity-sensitive dyes where, upon passing of a ski, a colour change of the chemical from violet to blue was claimed to be evidence of the presence of meltwater. Before the passing of the ski, no colour change took place. Afterwards, they observed a decrease in the red/blue ratio, with a higher temperature resulting in a greater blue shift, indicating the presence of meltwater and confirming the consensus that more water is present at higher temperatures.

Bäurle et al. [10] further stressed the importance of the real contact area in frictional behaviour. Using an X-ray computer tomograph, the real contact area was measured to be 6.4 % when a polyethene piston was pressed against a snow sample with snow grain size 500–1000 µm, at air temperature −10 °C and an apparent pressure of 30 kPa. This matches the magnitude of snow grain sizes measured by Lever [11] who saw grain size of 300–4000 µm for an apparent pressure of 70-100 kPa. Bäurle models the interaction of polyethene on ice with the FEM taking into consideration dry friction, heat conduction, phase changes, and the shearing of water films. For a polyethene slider with roughness similar to that of an ice sample, the temperature evolution will differ drastically, since the surface will be cooled intermittently when not in contact with the ice. For surfaces of similar roughness, a real contact area of 10 % was found to be a good match between simulation and experiment.

Findings by Kalliorinne [12] revealed that apparent contact length, a macro-scale parameter, had the greatest impact on friction, followed by total real contact area, which is a multi-scale parameter. For snow temperatures of −3 °C and −8.5 °C, a shorter apparent contact length resulted in a decrease in the coefficient of friction (COF). For this regime, it was concluded that the dominant frictional component might not be adhesive or abrasive friction. For temperatures colder than −13 °C, increasing apparent contact length L_a leads to a slight decrease in COF. This implies that factors related to L_a are more significant in determining COF in this regime. Kalliorinne attributes the decrease in COF for longer contact lengths at lower temperatures to a more uniform distribution of load across a harder snow surface, which diminishes the abrasive component of friction. This suggests that there is a shift in the balance between adhesive and abrasive friction mechanisms as the snow temperature decreases.

However, there is reason to be sceptical about the role that meltwater lubrication plays in the low friction of ice and snow. Experiments by Lever et al. [11] showed that snow grains could abrade rather than melt beneath polyethene sliders, even when prepared snow was given more time to sinter to create stronger bonds. Suggesting that abrasion can govern the kinetic friction of snow at low temperatures. For a nominal slider pressure of 0.8–3.6 kPa, a slider speed of 0.3–1.3 m s^{-1}, and a temperature range of −5 °C to −8 °C (measuring with an IR-camera), they saw no evidence of meltwater formation and the maximum temperature increase was only a few degrees, not close to melting. However, despite this, the measured friction coefficients were relatively low, ranging from 0.025 to 0.05. They attribute this to abrading snow particles filling in pore spaces, thereby smoothing the surface and reducing friction. In addition, using optical microscopy, it was found that the spots with the highest temperature were not contact points. Rather, the abraded particles found their way into the air pockets between the grains, which carried excess heat away from the interface. The authors conclude by saying that the heat conducted away from abrasion should be included in current friction models to identify the regimes for which self-lubrication is feasible. Examining the contact area, Lever found real contact areas ranging from 0.1–1.5 %. With a trend of increasing contact area for increasing temperatures. Although interesting, these findings, as Hasler [3] argue, are not entirely representative of actual skiing conditions.

Takeda et al. [13] found a behaviour similar to that of Lever where friction increased with increasing velocities until a crossover point of 0.5–1 m s^{-1}. Lever [11] speculated that the slider initially broke or abraded the relatively few static snow-grain contact points but then encountered higher resistance as abrasion increased the contact area. They saw a similar cut-off point of 0.5–1 m s^{-1}. Takeda, however, attributes this to the formation of meltwater at speeds higher than 1 m/s. It should be noted that Takeda

used an apparent pressure even lower than Lever of 0.8 kPa. Takeda also did not observe any noticeable pressure dependence at velocities of 0.1–1 $\mathrm{m\,s^{-1}}$ and pressures of 0.45–1.8 kPa. For static friction, longer contact times and smaller snow grain sizes led to higher static friction coefficients. Concluding that adhesion friction is the dominant static frictional component, as smaller snow grains develop a larger contact area, which increases the adhesive effect. They observed a greater effect of temperature on the static friction coefficient for 100 µm snow grains compared to 500 µm. As an explanation, they proposed that this was due to a liquid-like layer on the surface of the snow grains, which would have a higher adhesion force than solid ice, increasing in thickness with rising temperature. Takeda concludes by stating that "it seems that the attractive interaction force would arise from the dipole-induced dipole interaction. The dielectric constant of liquid water is far larger compared to that of solid ice, because the mobility of water molecules is far larger for liquid water. The attractive interaction energy of polyethene is expected to be larger with liquid water than with solid ice."

Molecular simulations by Atilla et al. [14] predict that ice surfaces can self-lubricate, even at very low temperatures (as low as −120 °C), caused by the shear forces that disrupt the crystalline structure, which creates a liquid-like zone that acts as a lubricant.

Weber et al. [15] have also studied the molecular interactions of sliding on ice and found that the slipperiness of ice is related to the mobility of surface molecules. Proposing that weakly hydrogen-bonded surface molecules diffuse in a rolling motion, which causes the slipperiness of ice.

Kietzig et al. [16] attribute the adhesive force of sliding friction to capillary bridges formed from meltwater, as proposed by Colbeck [17] and others. They found that a higher surface roughness increases the coefficient of friction of ice at low sliding speeds and temperatures well below the ice melting point, but at temperatures close to the melting point and at higher speeds, roughness and hydrophobicity significantly decrease ice friction. This would also explain why the hydrophobicity of the slider material reduces friction significantly in the mixed and hydrodynamic friction regimes. They also found that grooves in the slider, oriented in the sliding direction, also significantly decrease friction in the low velocity range compared to scratches and grooves randomly distributed over a surface.

Duncret et al. [18] wanted to examine the friction and abrasive wear of ultra high molecular weight polyethene (UHMWPE), the material used for ski bases, when sliding on ice. By defining an attack angle of the asperities of the ice surface, it was found that there is a substantial difference in the friction coefficient for small variations in the attack angle. In addition, the abrasive wear of UHMWPE in contact with ice is detectable.

The thermodynamic situation regarding frictional warming of snow and ice is complicated, and simplifications are often necessary. Evans, Akkök, Colbeck, Bäurle, Persson, and others have attempted to model this [19, 17, 10, 20]. Evans et al. [19] and later Akkök [21] derived an expression for a thermally controlled friction coefficient. Upon reaching a threshold temperature, the friction coefficient will depend only on the pressure and velocity of the sliding. They found a good match with the experiment for certain regions. Akkök also hypothesised that the threshold temperature could be below 0 °C, which means that melting does not take place and that some other mechanism is at play. If a water film is present, Persson [20] claims a thickness of only 10 Å would produce a low friction coefficient of ~ 0.02. However, this assumes full film lubrication, which in practice rarely occurs, if ever, in skiing [7, 8].

Whether the friction of snow and ice can be used interchangeably appears to be unclear. Lever [11] argues that ice and snow have different properties and therefore drawing conclusions from each other should be done with great care. Bowden [1], however, claims that they are very similar, with the main difference being the ploughing effect of snow.

Interestingly, Lehtovaara [22] found that low frequency vibration reduces kinetic friction of plastics sliding on ice at temperatures lower than −1 °C. The reducing effect was greater at −13 °C compared to −2 °C. They concluded that the vibrations can reduce the ploughing or change the contact area at the surface level.

1.2 Problem Statement

Whether the formation of frictional meltwater is the primary friction-reducing mechanism in the ski–snow contact remains unclear. Due to the complex nature of snow and ice, several friction-reducing mechanisms are likely involved. While substantial evidence supports the presence of a meltwater film, literature indicates that different mechanisms may dominate under different contact conditions. To better

understand these interactions, especially the role of meltwater, a more detailed analysis of the ski and snow interface, linking surface characteristics and material properties under actual skiing conditions, is essential.

1.3 Objectives

Utilising a Boundary Element Method (BEM) variational-based solver and an enthalpy-based phase change model, this work aims to investigate the conditions under which frictional heat dissipation leads to localised melting at the ski–snow interface. Specifically, the study will:

1. Determine the nature of the ski–snow contact and how it affects meltwater formation.
2. Analyse the influence of ski base textures, varying snow topographies, stiffness, and material properties on melting mechanisms.
3. Identify critical thresholds for meltwater formation under varying conditions.

1.4 Delimitations

This work is concerned only with the process of meltwater formation through frictional heating. Wear processes known to play a role in the ski–snow interaction, such as abrasion and ploughing [23][17], will not be considered. Due to this, the conditions that will be examined are equivalent to hard-packed snow and ice tracks at temperatures of $-5\,^{\circ}\mathrm{C}$ to $-15\,^{\circ}\mathrm{C}$, where the effects of wear and deformation are less pronounced.

Furthermore, hydrodynamic effects such as squeezing, along with more accurate methods for calculating the load capacity of the water film (Reynolds solver), will not be taken into account.

2 Method

This chapter presents the theoretical background, surface and material characterisation, and numerical approaches used in this thesis to investigate frictional melting at the ski–snow interface. The work is divided into three main components. First, the relevant physical theories governing contact mechanics, heat transfer, friction, and phase change are outlined. Second, the topographical and material properties of the ski and snow surfaces used in the simulations are described. Finally, the implementation of the numerical simulations, including both contact mechanics and heat conduction models, is detailed. These elements together form a multi-physics modelling framework aimed at capturing the dynamic interaction between a moving ski and a snow or ice surface under realistic conditions.

2.1 Theory

The theoretical framework underlying this thesis is grounded in models of surface contact, heat flow, and phase transition. The aim is to capture the essential physical mechanisms that govern meltwater formation due to frictional heating in the ski–snow contact. This section introduces the equations used to describe real contact area, energy balance at the interface, frictional heat generation in both dry and lubricated regimes, and the enthalpy-based modelling of phase change. These formulations serve as the foundation for the numerical simulations presented in later sections.

2.1.1 Contact Mechanics

An important variable in modelling the ski–snow contact is the real contact area. Due to the unevenness of the snow and ski surface, the actual contact area will be much less than the apparent contact area [17], see Fig. 2.

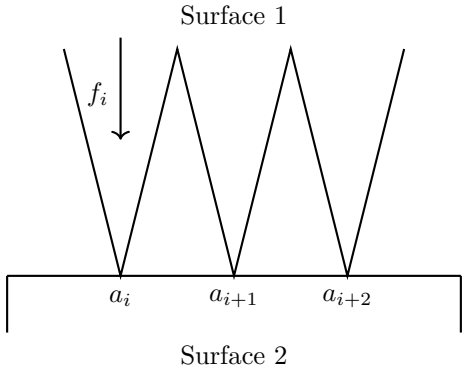

Figure 2: Microscopic contact between surface 1 and 2. $a_i, a_{i+1}, ...$ is the the area of each individual asperity. f_i is the load carried by asperity i.

The asperities that are actually in contact will carry all the load, which significantly affects the heat generated when modelling. According to Jacobsson [24], the real area of contact can be estimated by using the following reasoning: The total real contact area will be

$$A_{\mathrm{r}} = \sum a_i, \tag{2}$$

where $\mathrm{a_i}$ is the area of the individual contact spots. If the contact is purely plastic, then

$$a_i = \frac{f_i}{H}, \tag{3}$$

where H is the hardness of the softer material and $\mathrm{f_i}$ corresponds to the load of the contact spot i. Since the normal force is

$$F_{\mathrm{N}} = \sum f_i, \tag{4}$$

it follows that Equation (2) gives the real contact area as

$$A_{\mathrm{r}} = \frac{F_{\mathrm{N}}}{H}. \tag{5}$$

In this work, the real contact area is estimated using the numerical contact mechanics model described in Section 2.3.

2.1.2 Heat Flow and Energy Balance

When there is a temperature difference between surfaces, heat transfer must occur [25]. In the present work, conduction (heat transfer between solids in contact) is the primary consideration, because effects from convection will be low. This can be verified using the Nusselt number, which is a dimensionless number that quantifies the ratio of convective to conductive heat transfer. For a Nusselt number $Nu \lesssim 1$, heat is almost exclusively transferred by conduction. The Nusselt number is defined as

$$Nu = \frac{hL}{k}, \tag{6}$$

where h is the convective heat transfer coefficient, L is the characteristic length, and k is the thermal conductivity. Even when choosing a rather large characteristic length of $L = 500\,\mu\text{m}$, h would need to be unrealistically large for $Nu > 1$, which means that convective effects can be safely ignored.

At the ski–snow interface, the heat generated must be equal to the energy dissipated. Q_{friction} is the heat generated by friction, $Q_{\text{diffusion}}$ is the heat diffused into the snow, Q_{melt} is the heat required to melt, and Q_{snow} is the heat used to increase the temperature of the snow. This gives

$$Q_{\text{friction}} + Q_{\text{diffusion}} = Q_{\text{melt}} + Q_{\text{snow}}, \tag{7}$$

where

$$Q_{\text{friction}} = \mu P v t, \tag{8}$$

$$Q_{\text{diffusion}} = -k\frac{dT}{dz}, \tag{9}$$

$$Q_{\text{melt}} = \rho h L_f, \tag{10}$$

and

$$Q_{\text{snow}} = \rho h c_{\text{p}} \Delta T. \tag{11}$$

Substituting Equation (8)-(11) into (7) gives, after rearranging, the time t needed to generate a water film of thickness h as

$$t = \rho h \frac{c_{\text{p}}\Delta T + L_f}{\mu P v - k\frac{\Delta T}{d}}. \tag{12}$$

Equation (12) is later used to compare with the simulated results.

2.1.3 Modelling Dry, Lubricated, and Capillary Friction

As a ski passes over snow, heat will be generated due to friction. When there is no meltwater, in the dry regime, friction behaviour can be linked to deformations and fractures of the snow/ice asperities [8]. As a water film starts to develop, fewer and fewer of these asperities will be in contact, reducing the dry component of friction. According to Colbeck [8], the dry component of friction will decrease exponentially for increasing water film thickness h as

$$\mu_{\text{dry}} = \epsilon e^{-\xi h}, \tag{13}$$

where ϵ is the friction coefficient when no meltwater is present and ξ is a constant that depends on the properties of the snow/ice. Colbeck found good agreement with experiments when $\epsilon = 0.12$ and $\xi = 1 \cdot 10^6$.

Once a water film has developed, shear-induced viscous dissipation within the film leads to heat generation. In a Newtonian fluid, like water, the shear stress τ_{s} is proportional to the shear rate $\frac{\partial v}{\partial z}$ such that

$$\tau_{\text{s}} = \eta \left.\frac{\partial v}{\partial z}\right|_{z=0}, \tag{14}$$

where η is the viscosity of the fluid [25]. For planar Couette flow, see Fig. 3,

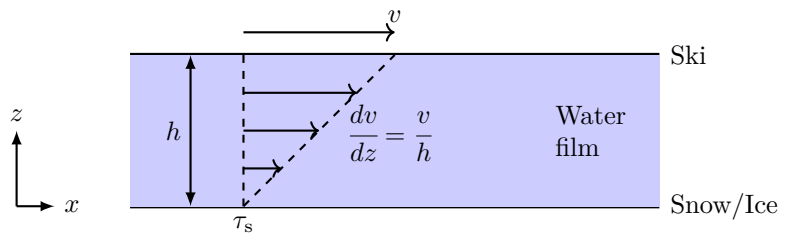

Figure 3: Planar Couette flow of the water film between the ski and the snow/ice.

the shear rate is simply

$$\frac{\partial v}{\partial z} = \frac{v}{h}. \tag{15}$$

Using (15) together with the following relations for shear stress τ_s and friction force f,

$$\begin{cases} \tau_\mathrm{s} = \dfrac{f}{A} \\ f = \mu_\mathrm{lub} F_\mathrm{N} = \mu_\mathrm{lub} P_\mathrm{N} A \end{cases}, \tag{16}$$

where P_N is the normal pressure placed on an asperity and A is the area of the contact (see Fig. 2), Equation (14) then gives the lubricated friction coefficient as

$$\mu_\mathrm{lub} = \frac{\eta v}{P_\mathrm{N} h}. \tag{17}$$

The behaviour of the capillary component is, according to Colbeck [8], not well understood. Nevertheless, by assuming that it scales with the cube of the film thickness, such that

$$\mu_\mathrm{cap} = \beta h^3, \tag{18}$$

Colbeck found that $\beta = 1.5 \cdot 10^{16}$ yielded good agreement with experimental data. For the thicknesses modelled, the capillary component will have the least effect.

Following Colbeck's approach, the dry and lubricated friction components can be combined by assuming they act in parallel, as in (mixed) elastohydrodynamic lubrication theory [8]. Accordingly, the total friction coefficient, accounting for capillary, dry, and lubricated contributions, can be expressed as

$$\mu = \mu_\mathrm{cap} + \frac{1}{\dfrac{1}{\mu_\mathrm{lub}} + \dfrac{1}{\mu_\mathrm{dry}}}. \tag{19}$$

Substituting Equation (18), (17), and (13) into (19) gives (when simplified)

$$\mu = \beta h^3 + \frac{1}{\dfrac{P_\mathrm{N} h}{\eta v} + \dfrac{e^{\xi h}}{\epsilon}}. \tag{20}$$

It can be seen that as h increases, μ will decrease, and if $h = 0$, $\mu = \epsilon$, which is the desired behaviour. An example is shown in Fig. 4.

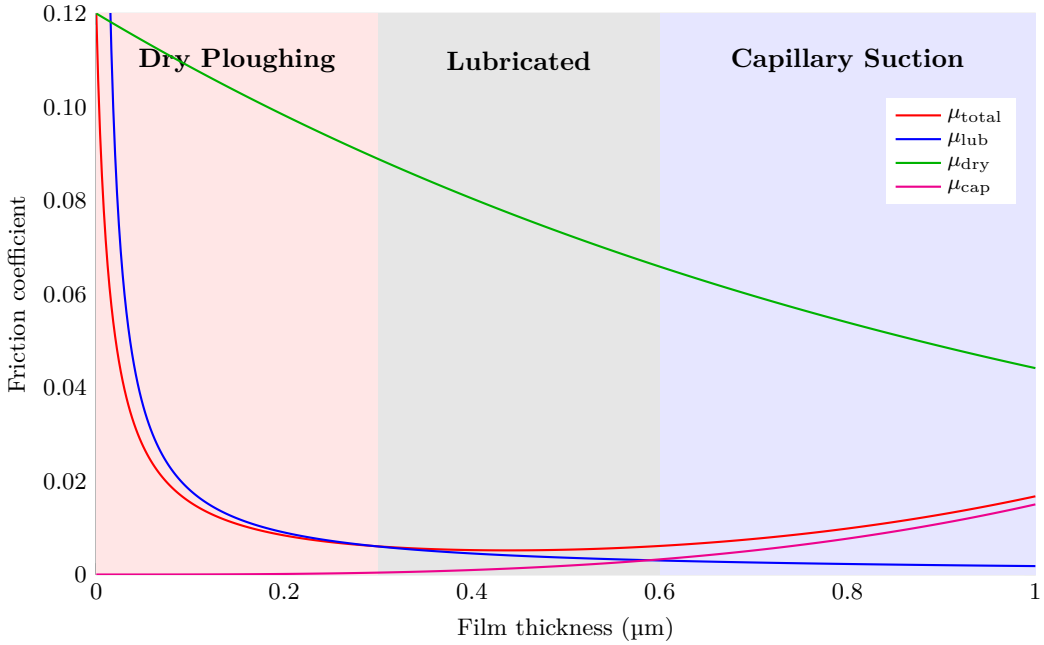

Figure 4: Visualisation of the behaviour of the dry and lubricated parts of the friction coefficients, assuming $\epsilon = 0.12$, $\xi = 1 \cdot 10^6$ and $\beta = 1.5 \cdot 10^{16}$, as suggested by Colbeck [8].

Lastly, as a skier experiences resistance due to friction, the heat dissipated will conduct downward into the snow or ice. The heat flux generated at the ski and snow interface is, according to [25], given by

$$q_{\text{friction}} = \mu P_{\text{N}} v. \tag{21}$$

Since Equation (20) represents the combined effect of capillary, dry, and lubricated friction, it can be substituted directly into Equation (8) to yield the total frictional heat flux.

2.1.4 Modelling Phase Change with an Enthalpy-Based Method

When snow is brought to a temperature of 0 °C, melting starts to occur. However, due to unevenness of snow grain size and air pockets within the snow, etc., melting occurs gradually. In the context of frictional heating at a ski–snow interface, the heat will propagate downward into the snow, creating a temperature gradient in which, given that the heat generated has raised the surface temperature to 0 °C, a region of partially melted and partially frozen snow, called a "slush" region, is speculated to appear, see Fig. 5.

Figure 5: Illustration of melting process, going from frozen snow, to a slush region and finally a fully melted water film.

To capture this effect, the source-based enthalpy method was chosen. The following method is based on the method described by Swaminathan [26]. The enthalpy evolution of the snow is governed by the heat equation.

$$\rho \frac{\partial H}{\partial t} = \nabla(k \nabla T), \tag{22}$$

where ρ and k are the density and thermal conductivity of the snow, respectively. H is the enthalpy of the system, defined as

$$H = c_{\mathrm{p}} T + g L_{\mathrm{f}}, \tag{23}$$

where c_{p} is the heat capacitance, L_{f} is the latent heat of fusion, and $0 \leq g \leq 1$, with $g = 0$ representing no melting and $g = 1$ complete melting. Using the source-based method, (23) can be substituted directly into (22), giving

$$\rho c_{\mathrm{p}} \frac{\partial T}{\partial t} + \rho L_{\mathrm{f}} \frac{\partial g}{\partial t} = k \nabla^2 T, \quad 0 < z < \infty, \quad t \geq 0, \tag{24}$$

as the thermal conductivity, k, is assumed to be constant within the snow/ice. In this case, the boundary conditions are given by Fourier's law of heat conduction at the surface, and the snow/ice at depth acts as a thermal reservoir at temperature T_{initial}, representing the undisturbed ground temperature

$$q_{\mathrm{friction}} = -k \left. \frac{\partial T}{\partial z} \right|_{z=0}, \quad T(\infty, t) = T_{\mathrm{initial}}. \tag{25}$$

Employing the explicit first- and second-order finite difference approximations (see e.g. [25]),

$$\frac{df}{dz} \approx \frac{f(z + \Delta z) - f(z)}{\Delta z}, \tag{26}$$

and

$$\frac{d^2 f}{dz^2} \approx \frac{f(z + \Delta z) - 2f(z) + f(z - \Delta z)}{(\Delta z)^2}, \tag{27}$$

and converting to index notation where $T_i^j = T(z_i, t_j)$ and $H_i^j = H(z_i, t_j)$, gives us an expression (based on equations (20), (8), and (25)) for the conduction-induced temperature increase in the z-direction as

$$T_1^j = T_2^j + \frac{\Delta z}{k} q_{\mathrm{friction}} = T_2^j + \frac{\Delta z}{k} \left(\beta h^3 + \frac{1}{\dfrac{P_{\mathrm{N}} h}{\eta v} + \dfrac{e^{\xi h}}{\epsilon}} \right) P_{\mathrm{N}} v, \quad \{j \in \mathbb{Z}^+\} \tag{28}$$

and an expression for the enthalpy (based on Equation (22)) of the following time iteration

$$H_i^{j+1} = H_i^j + \Delta t \frac{k}{\rho} \left(\frac{T_{i+1}^j - 2T_i^j + T_{i-1}^j}{\Delta z^2} \right), \quad \{(i, j) \in \mathbb{Z}^+\}. \tag{29}$$

The liquid fraction g gives three distinct regions. Solid, slush, and liquid.

1. **Solid:** Since the melting temperature has not been reached, no liquid will be present, hence $g = 0$. From Equation (23) this gives

$$\begin{cases} T = \dfrac{H}{c_{\mathrm{p}}} \\ g = 0 \end{cases} \tag{30}$$

2. **Slush**: When the temperature reaches the melting temperature, phase change will start to occur. During phase change, all energy will be used for the phase transition until it has exceeded the latent heat L_{f}. That is, the temperature will be constant. Accordingly, Equation (24) becomes

$$\rho L_{\mathrm{f}} \frac{\partial g}{\partial t} = \nabla(k \nabla T) \tag{31}$$

which, using the finite difference approximation gives[1]

$$\begin{cases} T = T_{\mathrm{melt}} \\ g = g_{\mathrm{old}} + \Delta t \dfrac{k}{c_{\mathrm{p}} L_{\mathrm{f}}} T_{zz}, \quad \{0 < g < 1\} \end{cases} \tag{32}$$

[1] Several methods for calculating g exist in the literature. Equation (32) for calculating g is different from the method described by Swaminathan [26] where g evolves over a certain temperature interval ΔT instead of $T =$ constant. The different methods for calculating g all gave very similar results.

3. **Liquid**: Fully melted region, $g = 1$

$$\begin{cases} T = \dfrac{H - L_{\mathrm{f}}}{c_{\mathrm{p}}} \\ g = 1 \end{cases} \tag{33}$$

The method can be summarised as illustrated in Fig. 6.

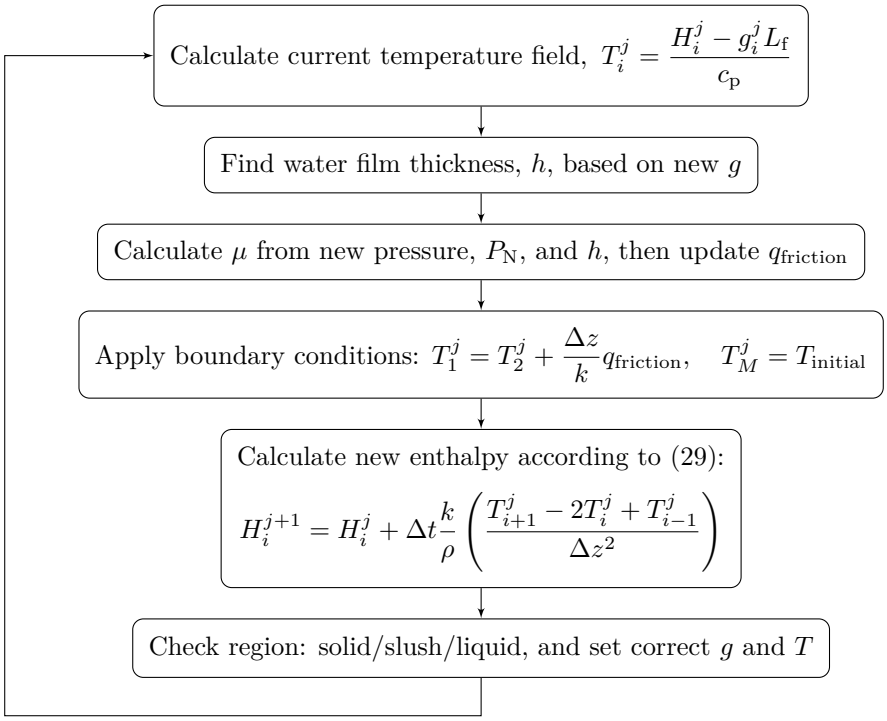

Figure 6: Flow chart of the enthalpy-based frictional melting simulation procedure. The model iteratively updates temperature and water film thickness based on energy balance and pressure-driven shear.

2.1.5 Stability Criteria for the Explicit Method

When simulating, the freedom to select Δz and Δt is desirable, as the balance between model accuracy and computing requirements needs to be controlled [25]. However, using the explicit time discretisation method, the solution is not unconditionally stable. That is, if Δz and Δt are set incorrectly, uncontrolled numerical oscillations will occur, giving non-physical solutions. To prevent this, Δz and Δt should be picked such that the Fourier stability criterion,

$$\mathrm{Fo} = \frac{k \Delta t}{c_p \rho (\Delta z)^2} < \frac{1}{2}, \tag{34}$$

is met. This follows directly from the discretised one-dimensional heat equation[2].

2.2 Surface Characterisation and Material Data

The following chapter provides definitions of important surface parameters used to define the snow and ski surface. The surfaces used in the simulations are presented in conjunction with a section on the material parameters.

2.2.1 Surface Roughness Parameters

Due to their irregular nature, surfaces are notoriously hard to define. However, an attempt can be made to do so using an increasing number of roughness parameters to better describe the surface of interest [27]. Since the objective of this thesis was not to draw direct correlations between these parameters and their frictional causation, a limited number of parameters were used. For our purposes, their usefulness lies in

[2] A full derivation and reasoning can be found in [25].

accurately modelling the correct order of magnitude of surface features, as well as being able to directly compare the roughness of the ski surface with that of the snow surface. The roughness parameters used and their definition are [28]:

I. S_a — *Average height deviation (above or below the mean plane) within the given reference area.*

$$S_a = \frac{1}{A} \iint_A |z(x, y)| \, dx \, dy$$

II. S_z — *Sum of the maximum peak height S_p, which is the mean of the 5 highest peaks, and the maximum valley depth S_v, which is the mean of the 5 deepest valleys, within the given reference area.*

$$S_z = S_p + S_v$$

2.2.2 Ski–Base Surface Topography

Although appearing rather smooth on the macro scale, the micro-scale topography of ski-base surfaces exhibits ridges, grooves, and general unevenness. Some of these features are desirable, purposely created to improve the glide qualities of a ski, while others are a result of the UHMWPE material structure, which is the material used for ski bases [18].

To investigate the effect of the micro-scale surface topography on contact characteristics and frictional melting, two representative ski-base textures, referred to as Linear 1 and Linear 3, from Kalliorinne et al. [7] were selected. Linear 1 represents a surface with low roughness, while Linear 3 has comparatively high roughness. These textures are typically used for different snow conditions and are therefore expected to highlight the influence of surface structure on frictional behaviour. The corresponding surface topographies are shown in Figs. 7 and 8, with their respective roughness parameters listed in Tables 1 and 2.

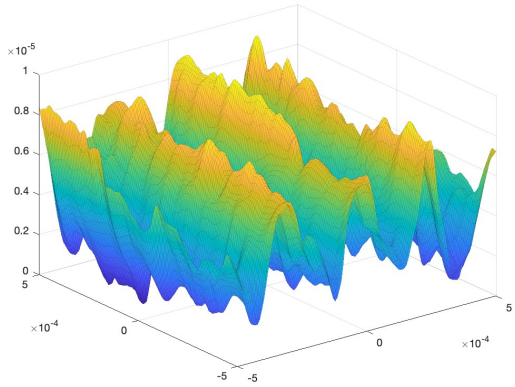

Figure 7: Linear 1 ski–base surface

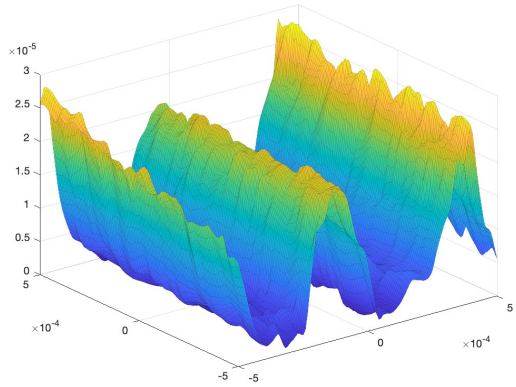

Figure 8: Linear 3 ski–base surface

Table 1: Roughness parameters for Linear 1

Surface	S_a	S_z
Linear 1	1.7547 µm	9.3711 µm

Table 2: Roughness parameters for Linear 3

Surface	S_a	S_z
Linear 3	6.813 µm	29.213 µm

2.2.3 Snow- and Ice Surface Topography

Snow is a complex material that shows very different characteristics depending on factors such as snow temperature, density, strength, liquid-water content, and crystal type [17]. In addition, when a ski passes over snow, it transforms. Flattening snow grains, deforming and abrading the surfaces, as well as causing ice crystallisation when meltwater refreezes.

Experiments by Hasler et al. [29] showed that the roughness of snow varied between $S_a = 163 - 185\,\mu\text{m}$ before the passing of a ski and $S_a = 6.2 - 74\,\mu\text{m}$ after one or more runs for snow temperatures between

$-1.3\,^{\circ}\mathrm{C}$ and $-19.1\,^{\circ}\mathrm{C}$, with higher temperature leading to a lower S_a. This is similar to the measurements performed by Bäurle et al. [10] of snow and ice that had not been compressed by skis. Based on these findings, surfaces were generated using a fractal surface generator developed by Andreas Almqvist [30]. Three surfaces were generated with varying roughness, rough, fine, and finer. Fig. 9 shows the fine surface. The surfaces finer and rough are the same as fine, but scaled down or up. Figures of these surfaces can be found in the Appendix section. The roughness parameters for all surfaces can be found in Table 3.

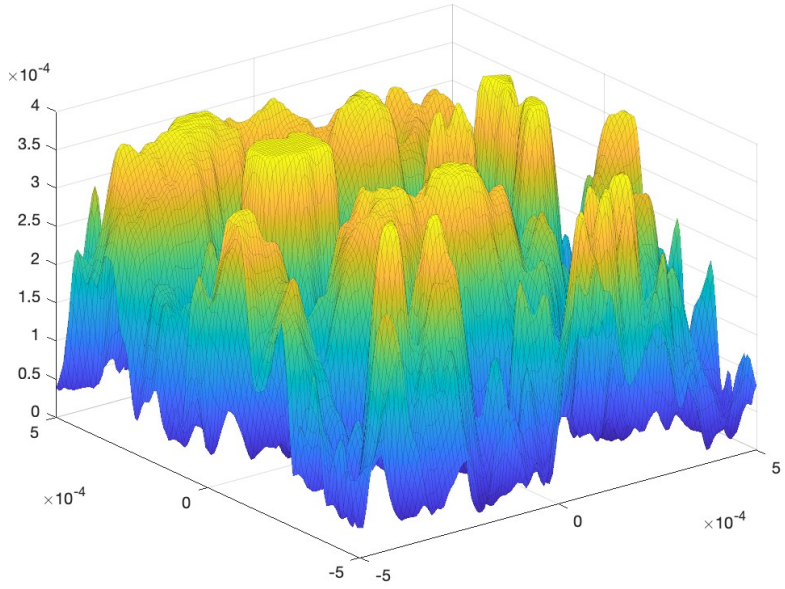

Figure 9: Fine snow surface

Table 3: Roughness parameters for snow/ice surfaces

Surface	S_a	S_z
Rough	48.418 µm	188.69 µm
Fine	5.5335 µm	21.564 µm
Finer	0.276 67 µm	1.0782 µm

2.2.4 Material Properties for Contact and Thermal Modelling

The hardness of the snow surface is the resisting force when a rigid body is pressed against the snow [31]. Two important determining variables are snow temperature and density. During all simulations, the density of the snow was taken to be $\rho = 550\,\mathrm{kg\,m^{-3}}$, which represents very hard ski tracks. Takeuchi [31] found that the hardness of snow at $-3\,^{\circ}\mathrm{C}$ varied according to

$$H_{\mathrm{snow},\rho} = 1.3 \cdot 10^{-10} \cdot \rho^4. \tag{35}$$

Using the relation $\frac{dH}{dT} \approx -3$ found by Tusima [32] for snow with density $\rho = 550\,\mathrm{kg\,m^{-3}}$, together with Equation (35), the following approximate expression can be extrapolated

$$H_{\mathrm{snow}} = -3.00T + 2.30. \tag{36}$$

Equation (36) gives hardness in terms of 10^5 Pa. For ice, Makkonen [33] found the following relation between hardness and temperature:

$$H_{\mathrm{ice}} = -5.08T - 15.19 \tag{37}$$

Equation (37) gives the hardness in terms of MPa. The hardness expressions are plotted in Fig. 10. The ski–base hardness was taken to be $H_{\mathrm{ski}} = 100\,\mathrm{MPa}$ (unmodified UHMWPE) [34].

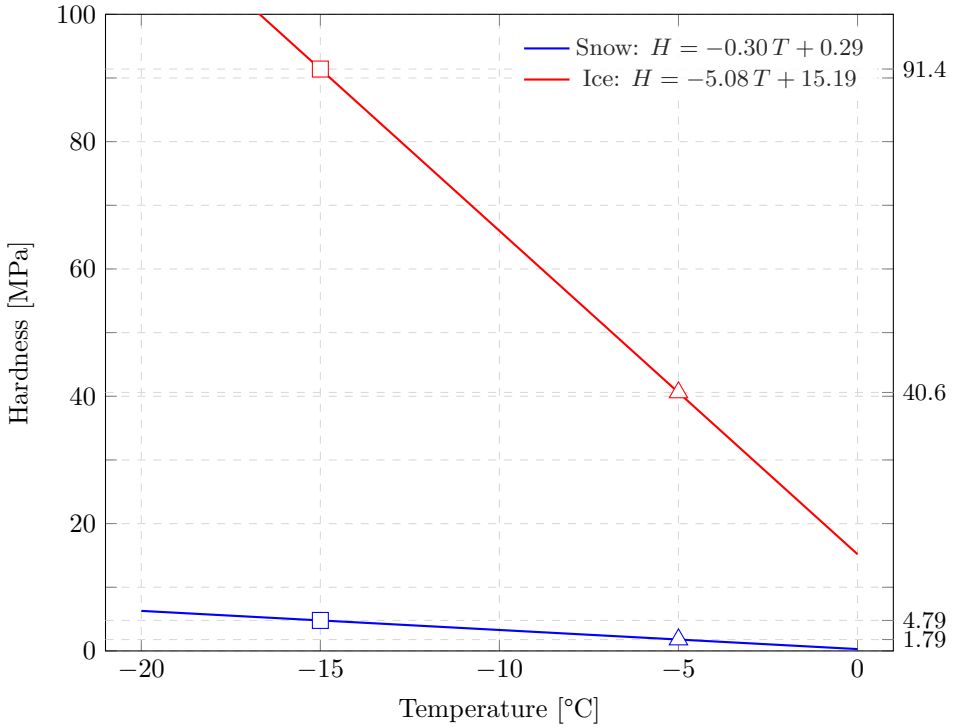

Figure 10: Hardness of ice (red line) and snow (blue line) with density $\rho = 550\,\mathrm{kg/m^3}$ for different temperatures within the range −20–0 °C. Triangles and squares represent the hardness at the simulated temperatures −5 °C and −15 °C, respectively.

Similarly, the elastic modulus of snow is also density- and temperature-dependent, where higher density and lower temperature generally lead to higher elastic modulus [35]. Lintzén [36] found that the elastic modulus of old snow is lower compared to newer snow for the same density and temperature. The elastic modulus of ice is on the order of 0.9 GPa and it increases with decreasing temperature [37]. For the ski base, the same elastic modulus, $E = 900\,\mathrm{MPa}$, as used by Kalliorinne [7] and corroborated by [34], was also employed here. In connection with this, a Poisson's ratio of $\nu = 0.3$ was assumed for the ski base, snow, and ice, although the ski-base material (UHMWPE) typically exhibits a slightly higher value.

The thermal conductivity, k, and capacitance, c_p, vary mainly (for our purposes) with temperature. Due to the bulk of the simulated region being snow, the ice surfaces were set with the same thermal conductivity as the snow. The heat transfer processes in snow are more complex than in ice. However, thermal conductivity is known to increase with increasing density and temperature [38]. Holmgren [39] derived the following expression for the thermal conductivity at −15 °C

$$k = 0.138 - 1.01\rho + 3.233\rho^2, \tag{38}$$

which for $\rho = 550\,\mathrm{kg\,m^{-3}}$ gives $k = 0.56$. The heat capacitance is the same for snow and ice. Table 4 gives a full list of the material data used in the simulations.

Table 4: Material data used in simulations. NA represents unused parameters.

Material	ρ (kg/m^3)	T (°C)	H (MPa)	E (MPa)	ν	k (W/m · K)	c_p (J/kg · K)
Ski base	NA	NA	100	900	0.3	NA	NA
Snow −5 °C	550	-5	1.79	130	0.3	0.62	2027
Snow −15 °C	550	-15	4.79	160	0.3	0.56	1972
Ice −5 °C	900	-5	40.6	9000	0.3	0.62	2027
Ice −15 °C	900	-15	91.4	9500	0.3	0.56	1972

Note that the exact parameter values for snow and ice are not what is important. What is important is ensuring that the parameter values are selected so that they accurately represent the known behaviour of

their respective material. For example, increasing hardness at lower temperatures or increasing thermal conductivity at lower temperatures for ice. In this way, general conclusions can be drawn regarding meltwater generation under different conditions.

2.3 Numerical Simulation

This section outlines the methodology used in the numerical simulations. Separate contact-mechanics simulations (CMS) and thermodynamic simulations were conducted to establish suitable input conditions for the friction-melting simulations (FMS), which are central to investigating the mechanisms of friction-induced melting. This division also helped reduce the overall computational cost.

2.3.1 Contact-Mechanics Simulations (CMS)

As the primary objective of this thesis is to investigate friction-induced melting mechanisms, a contact-mechanics solver based on a variational formulation, originally developed by Almqvist et al. [40][3], was employed in the present work. The solver considers elastoplastic contact between the surfaces, where the points exhibiting plastic yield are assumed to cause permanent deformation in the softer material. For example, if the ski is harder than the snow, the snow is deformed; conversely, if the counter-surface is harder, such as a compacted ice layer, the ski-base surface may be deformed instead. As the extent of plasticity increases, the contact area will approach the value given by Equation (5). Although the solver supports modelling of wear processes, this functionality was disabled for simplicity in the present simulations.

Due to the many possible choices for parameter values, having as many as possible constant over every simulation while still accurately modelling the given condition, is desirable. One of these is the simulated load on the skis. It was imagined that a skier with weight m_{skier} distributes their weight evenly over the total area of the glide zones A_{total}. This is a simplification, as in reality, $\sim$80 % of the skier load is distributed at the back of the heel [6]. The fractional load placed on the ski surface sample, with area A_{sample}, can then be obtained by

$$F_{\text{sample}} = \frac{A_{\text{sample}}}{A_{\text{total}}} F_{\text{total}}, \tag{39}$$

where

$$F_{\text{total}} = m_{\text{skier}} g, \tag{40}$$

and g is the gravitational acceleration.

The parameters g, A_{total}, A_{sample}, v_{ski}, representing the speed of the ski, m_{skier}, N, which is the number of grid nodes in the x- and y-directions and L_x, representing the domain length and width ($A_{\text{sample}} = L_x^2$) were kept constant for all contact mechanics simulations. These parameters, along with their values, are listed in Table 5.

Table 5: Constant parameters for all contact-mechanics simulations.

g [m/s^2]	A_{total} [m^2]	A_{sample} [m^2]	v_{ski} [m/s]	m_{skier} [kg]	N	L_x [m]
9.82	$16 \cdot 10^{-3}$	10^{-6}	5*	80	127	10^{-3}

* The nominal ski velocity is $v_{\text{ski}} = 5\,\text{m/s}$, except in specific simulation cases (see Table 6) where it is increased to 10 m/s.

To obtain a diverse set of data representing different conditions and the affects on the ski–snow interaction, the surfaces and material data of Sections 2.2.2, 2.2.3, and 2.2.4 were combined as listed in Table 6. Each simulation is identified using a structured naming convention: material type (snow = 'S', ice = 'I'), temperature (5 for $-5\,^\circ$C, 15 for $-15\,^\circ$C), ski-base topography ('L1' for Linear 1, 'L3' for Linear 3), followed by optional modifications. These include altered snow/ice roughness ('F1' for finer, 'F2' for fine, and 'R' for rough), increased elastic modulus ('E200' for $E = 200\,\text{MPa}$), repeated surface passes ('MP2' for two passes, 'MP5' for five), and increased skier velocity ('v10' for $v_{\text{ski}} = 10\,\text{m/s}$). When such a modification is present, all other parameters remain unchanged.

[3] This modelling framework has been furthered and utilised in several related studies, e.g., [41, 42, 43, 44, 45, 46, 7]

Table 6: Contact-mechanics simulation cases grouped by snow/ice condition. Identifiers indicate surface, temperature, and applied modification as described in the text.

Condition	Identifier	Ski Surface Topography	Snow/Ice Surface Topography
Snow −5 °C	S5L1F2	Linear 1	Fine
	S5L3F2	Linear 3	Fine
	S5L1R	Linear 1	Rough
	S5L1F2E200	Linear 1	Fine
	S5L1F2MP5v10	Linear 1	Fine
	S5L1F2MP2	Linear 1	Fine
Snow −15 °C	S15L1R	Linear 1	Rough
	S15L3R	Linear 3	Rough
Ice −5 °C	I5L1F2	Linear 1	Fine
	I5L3F2	Linear 3	Fine
	I5L1F2MP2	Linear 1	Fine
	I5L1F2MP2v10	Linear 1	Fine
Ice −15 °C	I15L1F1	Linear 1	Finer
	I15L3F1	Linear 3	Finer
	I15L1F1MP2v10	Linear 1	Finer
	I15L1F2	Linear 1	Fine
	I15L1R	Linear 1	Rough

Obviously, in real-life skiing, when a ski passes over a snow or ice asperity, there is not just one contact event but many, as the entire length of the ski passes over the same spot. However, computational limitations restricted the simulations to a maximum of five periodic passes of the ski surface over the snow or ice. To investigate the effect of refreezing between asperity contacts and the evolution of the water film upon recontact, two passages were typically simulated. In addition, the sliding speed was increased from $5\,\mathrm{m\,s^{-1}}$ to $10\,\mathrm{m\,s^{-1}}$ in selected cases to emulate high-speed skiing.

In the context of this study, a simulation *run* refers to a single simulation case defined by a unique combination of parameters from Tables 5 and 6. With these inputs, the solver iteratively finds the load balance at each time step, then advances one Δx, repeating this process for one or multiple passages over the domain length L_x, depending on the run. An example is shown in Fig. 11, which in (a) depicts the contact between the ski base surface and snow, and in (b) the corresponding pressure distribution at an intermediate time step.

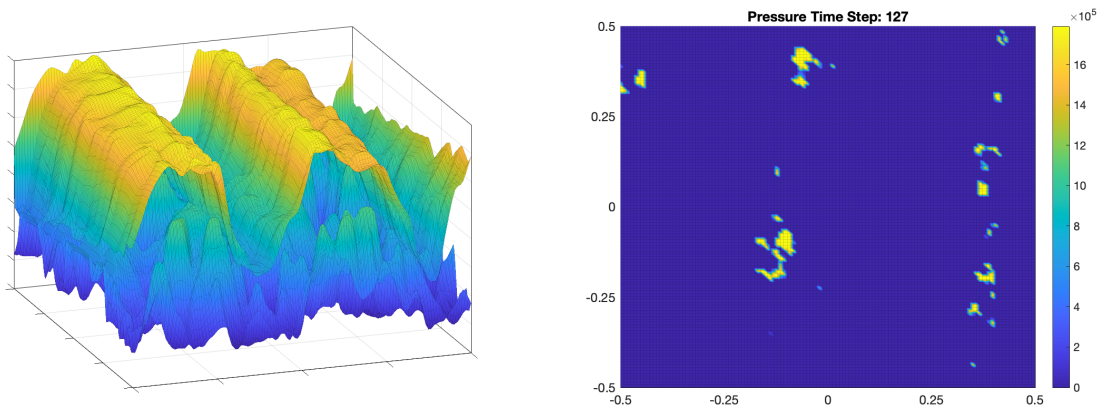

(a) (b)

Figure 11: (a) Ski and snow/ice surfaces in contact. (b) Corresponding pressure distribution at a selected time step, both produced by the contact mechanics solver.

After the solver has iterated through each time step, the resulting contact data is post-processed through a custom function that tracks each individual node. This function determines the longest contact duration and calculates the average contact duration across all nodes. The outputs generated include the total contact area, a pressure histogram for all contacts, and node-specific time–pressure data for key locations, such as the node with the longest contact, the average-contact node, the node with the highest energy, and one exhibiting an early sharp pressure rise. These results serve as input to the subsequent friction-melting simulations, which are performed using the enthalpy-based method.

2.3.2 Friction-Melting Simulations (FMS)

To simulate the development of meltwater films caused by frictional heating at the ski–snow interface, a one-dimensional finite difference model was developed. This model uses the enthalpy-based phase change formulation described in Section 2.1.4 and is initialised with data from the CMS.

Each FMS was conducted in a one-dimensional domain in the depth (z) direction, extending from the snow surface to the bulk. The spatial domain was discretised using a finite difference grid of length L_z, subdivided into N_z equally spaced nodes. The bottom boundary of the domain was maintained at the initial snow or ice temperature (either $-5\,^\circ\mathrm{C}$ or $-15\,^\circ\mathrm{C}$), simulating the thermal reservoir effect of deeper snow. The top boundary represented the snow surface directly beneath the ski, where the friction-induced heat output was applied.

To ensure numerical stability, the time step Δt and spatial step Δz were chosen to satisfy the Fourier stability condition, with Fo given by (34), for explicit time integration.

In all simulations, Fo ≈ 0.5 was targeted for maximum spatial resolution while maintaining stability.

The vertical domain size L_z was chosen based on the thermal penetration depth:

$$\delta = \sqrt{\frac{k}{\rho c_p} t}, \tag{41}$$

where t is the characteristic contact time. For typical conditions (e.g., $k = 0.62\,\mathrm{W/m{\cdot}K}$, $\rho = 550\,\mathrm{kg/m^3}$, $c_\mathrm{p} = 2027\,\mathrm{J/kg{\cdot}K}$, $t = 200\,\mu\mathrm{s}$), this yields $\delta \approx 10\,\mu\mathrm{m}$, which was used as the domain height in all simulations.

The initial temperature profile was uniform and equal to the ambient temperature of the snow or ice. During contact, the top boundary received a heat flux from frictional heating, computed as

$$q_\mathrm{friction} = \mu(t) P_\mathrm{N}(t) v, \tag{42}$$

where $\mu(t)$ is the effective friction coefficient, evolving dynamically with the local meltwater thickness $h(t)$ according to Equation (20), $P_{\mathrm{N}}(t)$ is the interpolated normal pressure from the CMS, and v is the skier's velocity. The resulting heat flux was applied to the top node via Fourier's law. The simulation setup is illustrated in Fig. 12a, while a typical result showing the temperature evolution over time is presented in Fig. 12b.

After the contact event ended, a zero-flux condition was applied to the top node, simulating the removal of the heat source. This allowed the model to capture the natural cooling and refreezing behaviour of any remaining meltwater.

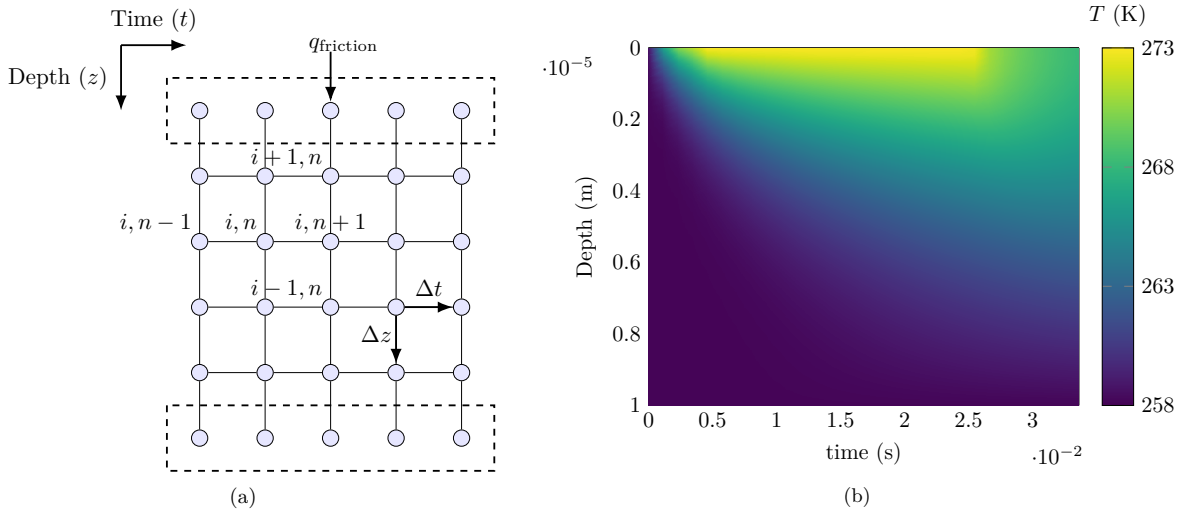

Figure 12: (a) Schematic of the spatial discretisation used in the FMS simulations. (b) An example of a simulated temperature profile over time following application of frictional heat flux.

At each time step, the enthalpy of each node was updated according to Equation (29). The updated enthalpy values were then used to calculate the new temperature and liquid fraction g using the phase-dependent relations outlined in Section 2.1.4. This approach captured the solid, slush, and liquid regimes as the simulation progressed.

The simulation used pressure and duration data from selected contact points in the CMS. To allow an appreciable amount of meltwater to develop, the node with the longest contact duration was chosen in each simulation case. The CMS pressure output was interpolated to match the FMS time step and used in Equation (42). For simulations involving repeated contact (e.g., MP2 or MP5), the contact (heating) phase was separated by periods of zero pressure to allow partial refreezing.

For each simulation, the following outputs were recorded:

- Maximum meltwater film thickness, $h_{\max}$.
- Time at which $h_{\max}$ occurred.
- Refreezing duration, defined as the time needed for the meltwater film to completely freeze after the final contact.
- Temperature and enthalpy profiles over time and depth (see Fig. 12b for an example).

The overall friction melting simulation process consisted of the following steps:

I. Pre-processing:
   - Load contact pressure and duration data from CMS.
   - Interpolate pressure to match FMS time step.

II. Initialisation:
   - Set initial temperature and enthalpy profiles.
   - Determine simulation grid dimensions and parameters.

III. Time integration loop (see Fig. 6 for more detailed steps):

- Compute frictional heat flux at the surface.
- Update enthalpy and resolve phase state (solid, mushy, liquid).
- Track meltwater film thickness over time.

IV. Post-processing:

- Extract relevant meltwater and temperature metrics.

The decision to combine Frictional Melting Simulations (FMS) with Contact Mechanics Simulations (CMS) was motivated by the requirement to capture both the mechanical and thermal aspects of ski–snow interaction under realistic conditions. While empirical measurements (e.g., temperature sensors or high-speed imaging) provide valuable data, they lack the resolution and control necessary to isolate the effects of multiscale topography and material properties. Similarly, purely thermal or simplified tribological models do not adequately represent the pressure-dependent and surface-roughness-dependent contact mechanics that dominate at sub-zero temperatures. By integrating FMS and CMS, the model captures the dynamic feedback between pressure distribution, contact area, and heat generation, making it particularly suited for assessing meltwater formation and refreezing phenomena in cold conditions.

3 Results and Discussion

This section presents the results of the coupled Contact Mechanics Simulations (CMS) and Frictional Melting Simulations (FMS), which were performed to investigate meltwater film generation at the ski–snow and ski–ice interface under realistic skiing conditions. The simulations span a range of surface textures, snow/ice types, and ambient temperatures ($-5\,^{\circ}\mathrm{C}$ and $-15\,^{\circ}\mathrm{C}$).

Each simulation is identified using a shorthand code, such as S5L1F2, where 'S' denotes snow, '5' the (absolute) temperature, 'L1' the ski base texture, and 'F2' the counter surface topography. The main outputs include meltwater film thickness, refreezing times, and contact pressures, and are compared with analytical estimates based on Equations (12) and (5). A summary of all simulation results is provided in Table 7.

The subsections that follow offer a breakdown of the key findings, a discussion of emerging patterns, and an examination of representative simulation cases.

3.1 Summary of Simulation Outcomes

Table 7 summarises the numerical results. For each simulation case, the table reports:

- The maximum meltwater film thickness and time of occurrence
- Calculated melt times for the reported film thickness
- Refreezing duration after contact
- Longest and average contact durations
- Mean pressures during contact (for both longest and average durations)
- Simulated and calculated contact area (CA)

Entries marked as N/A indicate simulations that were not performed, or where the melt layer was negligible, making metrics like refreeze time irrelevant. Runs involving repeated contact (e.g., MP2 or MP5 variants) were treated with intermittent pressure-free intervals to allow partial refreezing. This behaviour is modelled explicitly in the FMS and results in more complex time histories.

Table 7: Summary of simulation results for the CMS and FMS.

Condition	**Identifier**	**Max. film thick.** [nm]	**Time max. thick.** [µs]	**Calculated time** [µs]	**Time refreeze** [µs]	**Longest contact** [µs]	**Mean press. (long)** [MPa]	**Avg. contact** [µs]	**Mean press. (avg.)** [MPa]	**Mean CA** [%]	**Calculated CA** [%]
Snow −5 °C	S5L1F2	44.8	46.8	27.2	21.1	75.6	1.44	12.6	1.42	1.80	1.37
	S5L3F2	29.9	21.7	12.7	6.23	39.4	1.47	6.30	1.51	1.60	1.37
	S5L1R	59.7	63.2	39.4	27.0	89.8	1.56	15.7	1.36	1.72	1.37
	S5L1F2E200	44.8	46.8	22.6	23.9	64.6	1.60	11.0	1.56	1.68	1.37
	S5L1F2MP5v10	89.6	N/A	N/A	124	N/A	N/A	N/A	N/A	N/A	N/A
	S5L1F2MP2	44.8	46.6	19.7	19.1	N/A	N/A	N/A	N/A	N/A	N/A
Snow −15 °C	S15L1R	29.9	40.5	16.7	N/A	175	3.28	18.9	2.86	0.83	0.51
	S15L3R	29.9	20.2	5.87	N/A	44.1	4.39	9.45	3.97	0.64	0.51
Ice −5 °C	I5L1F2	119	94.0	56.4	65.1	121	22.4	7.87	10.4	0.19	0.060
	I5L3F2	74.6	32.9	10.8	30.6	33.1	19.7	4.72	25.5	0.096	0.060
	I5L1F2MP2	119	N/A	N/A	74.0	N/A	N/A	N/A	N/A	N/A	N/A
	I5L1F2MP2v10	313	N/A	N/A	186	N/A	N/A	N/A	N/A	N/A	N/A
Ice −15 °C	I15L1F1	29.9	3.40	4.20	N/A	40.9	8.50	6.30	11.4	0.25	0.027
	I15L3F1	44.8	11.0	1.88	N/A	23.6	33.0	6.30	18.2	0.097	0.027
	I15L1F1MP2v10	75.0	N/A	N/A	60.0	N/A	N/A	N/A	N/A	N/A	N/A
	I15L1F2	59.7	119	19.2	N/A	123	32.0	7.87	9.22	0.18	0.027
	I15L1R	43.5	3.75	5.85	N/A	89.8	31.7	9.45	12.4	0.17	0.027

3.2 Interpreting Key Results

The results illustrate several key patterns:

- **Temperature dependence:** As expected, lower ambient temperatures generally reduced meltwater film thicknesses and shortened or eliminated refreezing periods due to reduced frictional heating and faster conductive cooling.
- **Material contrast:** Ice tests (e.g., I5L1F2) often produced thicker water films due to higher pressures and longer contact durations, compared to snow runs at the same temperature. This is consistent with analytical predictions based on Equations (42) and (12).
- **Surface texture influence:** Variations in ski base structure (e.g., L1 vs. L3) had a noticeable effect on contact area and pressure distribution. Finer structures tended to reduce localised peak pressure but increase contact duration, leading to longer melt-times and higher $h_{\max}$ values.
- **Repeated contact:** MP simulations revealed cumulative meltwater build-up and extended refreezing periods. For instance, I5L1F2MP2v10 yielded the largest observed film thickness, 313 nm, with a refreeze time of 186 µs.

3.3 Example Case References

The following sections analyse representative simulations in detail. References such as S5L1F2 or I15L3F1 are used consistently to identify test conditions, as encoded in the simulation labels. Figures accompanying each case highlight the spatial and temporal evolution of temperature, enthalpy, and meltwater thickness, illustrating how the underlying contact mechanics influence thermal behaviour.

The following sections provide a more detailed analysis of the results summarised in Table 7. The figures presented in the main text were selected to best illustrate the range of behaviours observed under different conditions.

3.4 Nature of the Ski–Snow Contact

In this section, unless otherwise mentioned, the analysis is made from the data in Table 7.

A clear trend is observed between the surface material and the contact area. Simulations on snow produce considerably larger real contact areas, reaching up to 1.80 %, compared to ice, where the contact area remains below 0.25 %. This behaviour is consistent with both the calculated values and the expectation that softer surfaces allow for increased plastic deformation, leading to larger contact areas. The calculated contact areas agree more closely with the simulations for snow than for ice, likely due to the increasing role of elastic contacts on harder surfaces. Looking at Fig. 14a, most pressures observed equal the snow hardness ($H_{\text{snow}} = 1.8$ MPa), indicating predominantly plastic contact. In Fig. 14b, pressure values are more evenly distributed relative to the ice hardness ($H_{\text{ice}} = 42$ MPa), suggesting that most contacts remain elastic.

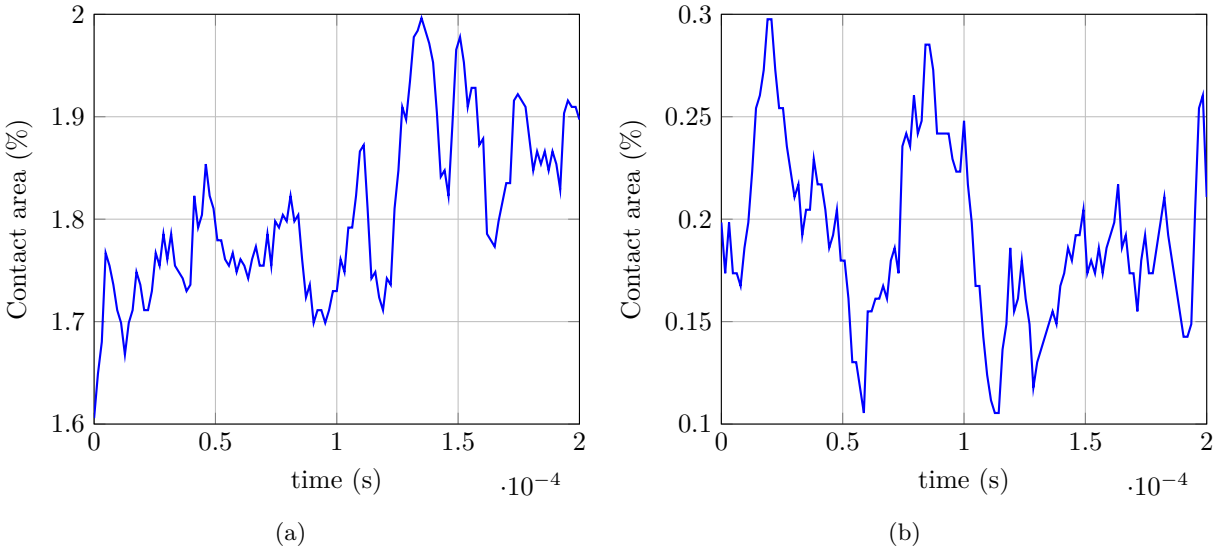

Figure 13: Contact area evolution over time for simulation runs (a) S5L1F2 and (b) I5L1F2.

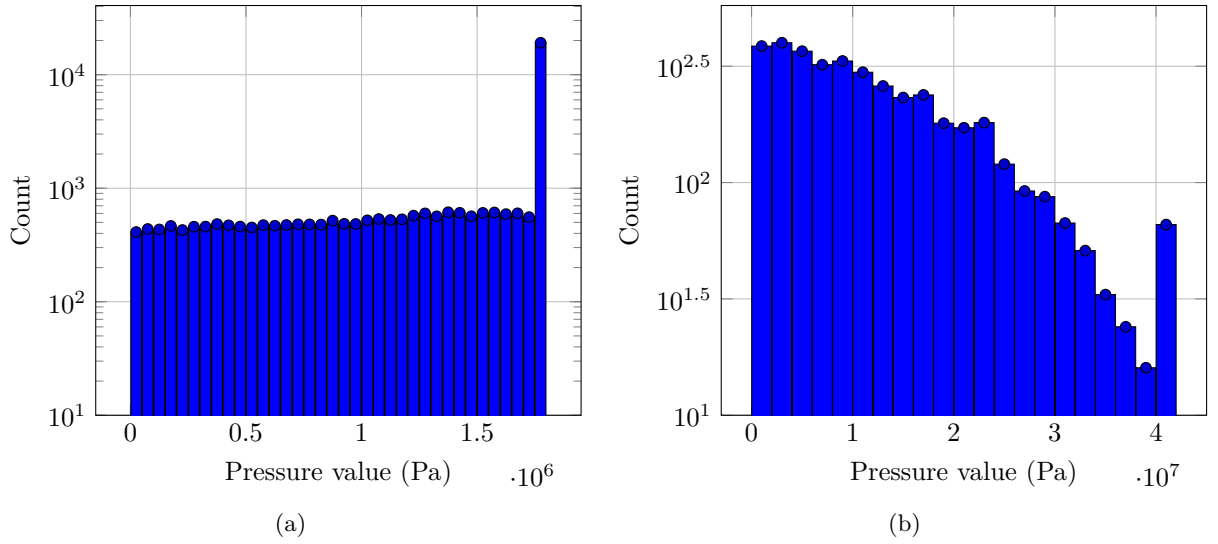

Figure 14: Histograms of non-zero pressure values for simulation runs (a) S5L1F2 and (b) I5L1F2.

As expected, an inverse relationship is observed between the contact area and the contact pressure. With a decreasing contact area, the remaining contacts must sustain a higher load, resulting in locally higher pressures. In S5L1F2, a contact area of 1.81 % corresponds to a mean pressure of 1.44 MPa, while in I5L1F2, with only a contact area of 0.192 %, the mean pressure increases to 22.4 MPa. In I15L3F1, the highest pressures were observed, exceeding 33 MPa. At the high pressures involved, the pressure-induced reduction in the melting temperature may become significant. However, this effect was not taken into account in the present work.

Another feature observed, primarily in the snow simulations, is the increase in contact area as the contact progresses over time. This can be seen in Fig. 13a. This effect was more pronounced for softer surfaces, such as snow. The underlying mechanism is attributed to plastic deformation. Softer materials deform more easily and allow the load to be distributed over larger areas, while harder surfaces primarily shift the load between individual asperities, maintaining localised pressure peaks.

The roughness of the snow and ice surface also has a clear influence on contact behaviour. Generally, increasing surface roughness results in longer maximum contact durations and slightly reduced contact areas. This is evident when comparing I15L1F1, I15L1F2, and I15L1R, as well as when comparing S5L1F2 and S5L1R. This behaviour can be explained by the increase in the number of peak-to-peak contacts with

higher roughness. These contacts deform snow and ice more easily, prolonging the duration of the contact but reducing the real contact area. As a consequence, in the simulations, rougher snow or ice surfaces are likely favourable for promoting meltwater generation due to the combination of longer contact times and higher localised pressures.

In contrast, increasing the roughness of the ski base results in a consistent decrease in both contact duration and contact area. As stated above, the snow and ice surface deforms while the ski base does not, which is why increased ski–base roughness leads to a decrease in contact time, not an increase like for snow and ice. The smoother Linear 1 texture consistently produces larger contact areas than the rougher Linear 3 texture. For example, comparing Runs S5L1F2 (Linear 1) and S5L3F2 (Linear 3) under identical snow and temperature conditions shows a decrease in the (relative) contact area from 1.81 % to 1.61 %. This trend persists across all material combinations and likely reflects better conformity between the ski and snow surfaces, as well as a more evenly distributed pressure over the contact plane.

The effects of temperature on the contact area follow the expected trend that lower temperatures generally reduce the contact area due to the increased hardness of the material. As shown in Fig. 10, the hardness of snow and ice increases with decreasing temperature. For example, going from ice at $-5\,^{\circ}\mathrm{C}$ (with $H = 40.6\,\mathrm{MPa}$) to ice at $-15\,^{\circ}\mathrm{C}$ ($H = 91.4\,\mathrm{MPa}$), the hardness doubles. However, the corresponding decrease in the simulated contact area is relatively small, suggesting that once the contacts are primarily elastic, further increases in hardness have a diminishing effect on the real contact area. Comparing the calculated CA with the simulated, at higher hardness, they diverge.

Lastly, when examining contact durations, the longest contact times are observed for a rough snow surface and the smoother Linear 1 ski-base, notably S15L1R (0.175 ms) and S5L1R (0.090 ms). In contrast, the shortest contacts occur on ice, especially in I15L3F1 (0.024 ms), where the high hardness and surface mismatch reduce the duration of contact. Average contact durations are generally an order of magnitude shorter than maximum values, indicating that most contact spots form and break rapidly during sliding. Longer contact durations increase the opportunity for heat accumulation at the interface, promoting local melting. However, short but intense contacts, as observed in the ice cases, can still generate significant localised heating because of extremely high pressures. This creates favourable conditions for meltwater formation even when bulk heating would otherwise be insufficient.

3.5 Meltwater Formation

This section analyses the meltwater formation observed in the simulations, its dependence on contact conditions, and the underlying mechanisms controlling its formation. The meltwater film results are obtained from the FMS, which uses contact data from the CMS as input. Various factors, such as surface topography, temperature, contact duration, pressure, and sliding speed, are examined to identify the governing mechanisms and thresholds for meltwater formation. Fig. 15 summarises the maximum meltwater generated in each case from Table 7. The results show that rougher ski surfaces (e.g. Linear 3) generally lead to thinner meltwater films, likely due to reduced contact area and shorter contact durations. In contrast, finer snow surfaces tend to promote slightly more meltwater formation than rougher ones. Lower ambient temperatures significantly reduce the generation of meltwater. Increased sliding speed and repeated contact cycles (MP2, MP5, v10) result in substantial meltwater generation, particularly on ice.

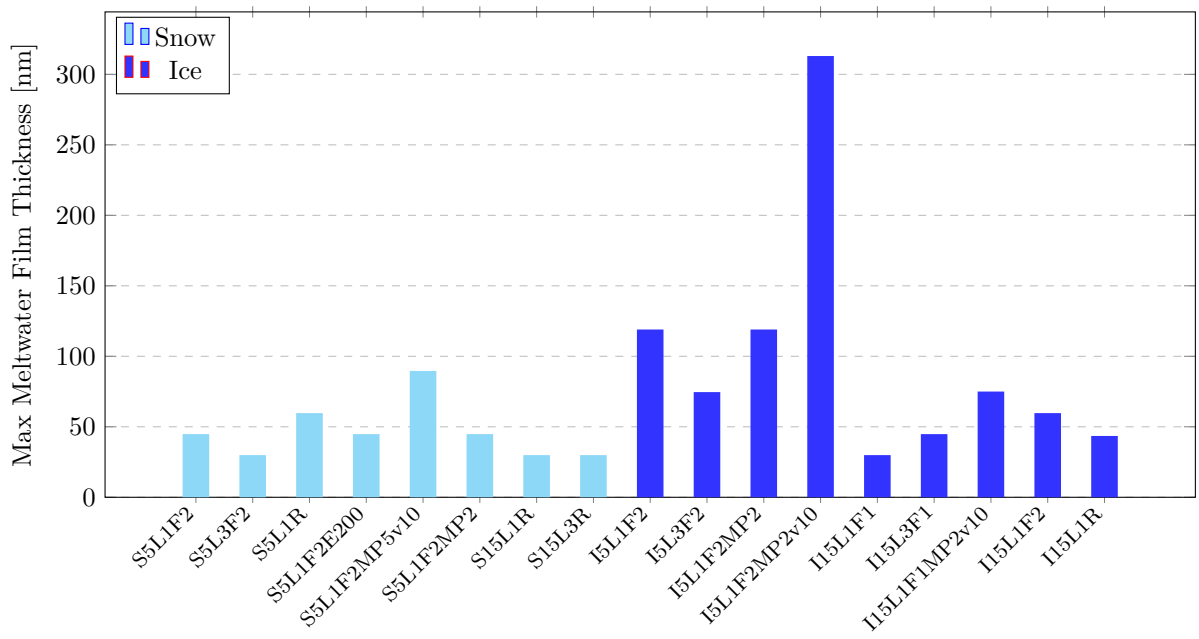

Figure 15: Maximum meltwater film thickness for all simulation cases, grouped by snow (cyan) and ice (blue) conditions.

3.5.1 General Meltwater Formation Trends

The maximum meltwater film thickness varied substantially across the simulated conditions, ranging from 30 nm to 300 nm (Fig. 15). For a given ski base roughness, the meltwater films were consistently thicker on ice surfaces than on snow. This is attributed to the significantly higher pressures in the ski–ice interface, which generate more frictional heat. For example, I5L1F2 (ice at $-5\,^{\circ}\mathrm{C}$) generated a film thickness of 119 nm, compared to only 44.8 nm for the corresponding snow case S5L1F2 under otherwise identical conditions, see Fig. 16. The highest meltwater thickness observed overall was for the case I5L1F2MP2v10, where increased sliding speed ($10\,\mathrm{m\,s^{-1}}$) and repeated asperity contacts resulted in a film of 313 nm.

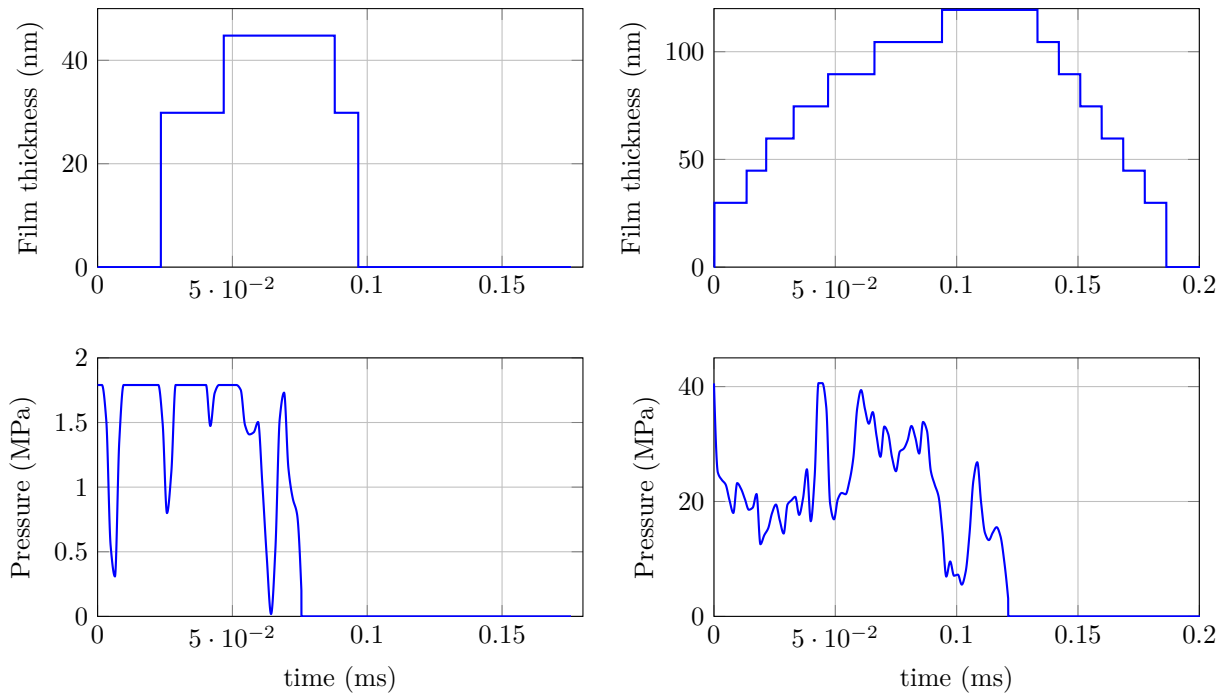

(a) (b)

Figure 16: Time evolution of meltwater film thickness (top) and contact pressure (bottom) for the simulation cases S5L1F2 (a) and I5L1F2 (b).

3.5.2 Effect of Snow and Ice Temperature

Temperature had a pronounced effect on meltwater formation. While meltwater still developed at −15 °C, the resulting film thicknesses were substantially lower than at −5 °C. For example, the case I15L1F1 generated a maximum film thickness of only 29.9 nm (Fig. 17a), compared to 119 nm for I5L1F2 under otherwise similar conditions (Fig. 16). When using the rougher Linear 3 ski base, a decrease from 74.6 nm to 44.8 nm was observed with decreasing temperature. The rougher Linear 3 ski base surface produced slightly more meltwater than Linear 1 at −15 °C, with intermittent peaks around 0.011 and 0.013 ms (Fig. 17b). This was, however, not the general trend, as Linear 1 consistently generated more meltwater under most other conditions. This deviation is discussed further in Section 3.5.3.

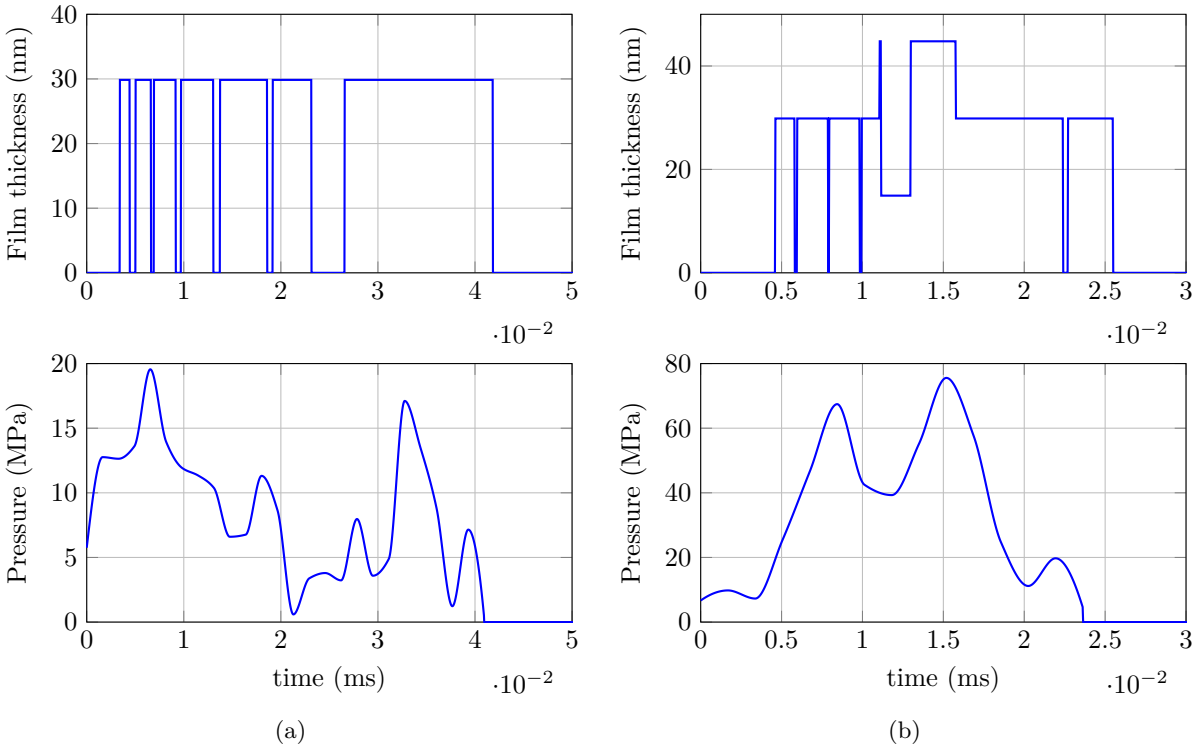

Figure 17: Time evolution of meltwater film thickness (top) and contact pressure (bottom) for I15L1F1 (a) and I15L3F1 (b), both simulated at −15 °C.

For snow, the effect of temperature was similarly pronounced. Simulations at −15 °C, specifically S15L1R and S15L3R, resulted in maximum meltwater film thicknesses of approximately 30 nm, whereas the corresponding case at −5 °C (S5L1F2) reached 44.8 nm. Despite the higher contact pressures observed at lower temperatures (due to increased snow hardness and reduced compliance), the resulting frictional heating was insufficient to produce thicker films. This indicates that, for snow in particular, the higher energy barrier to melting at colder temperatures outweighs any gain from increased local pressures.

As outlined in Section 2.2.4, both snow and ice hardness becomes harder as temperature decreases. This increase in hardness results in a reduced contact area and higher contact pressure, which in turn elevates local frictional heating. However, at lower temperatures, more energy is required to raise the material to its melting point. Consequently, despite higher pressures, the available frictional heat may still be insufficient to initiate melting. This trade-off between pressure-induced heating and the elevated energy barrier explains the overall reduction in meltwater formation observed under colder conditions.

3.5.3 Effect of Surface Roughness

Surface roughness affects meltwater generation primarily by altering contact area and duration. Simulations in which rougher snow or ice surfaces were used (for example, S5L1R, I15L1R, I15L1F2) showed longer maximum and average contact durations, but slightly reduced contact areas compared to S5L1F2 or I15L1F1, where finer surfaces were used. These longer contact times are likely related to how the snow or ice surface deforms. When using a rougher surface, less of the ski surface will be in contact, meaning that the contact points will have a higher pressure, possibly higher than the hardness of the snow or ice surface, which will then plastically deform the snow or ice.

As we have seen, material that deforms more easily (i.e. snow compared to ice) results in longer contact durations. These longer contacts allow for more time for heat to accumulate at individual asperities, thereby increasing the amount of meltwater generated. When investigating the influence of different snow types on the coefficient of sliding friction, Eriksson [47] found a decrease in kinetic friction for increasing snow grain size. According to Eriksson, skis glide faster on larger snow crystals than on newly fallen snow with a small grain size. Although somewhat speculative, this behaviour could be explained by the results of this thesis. That is, a rougher snow surface composed of larger grains could increase the duration of the individual asperity contacts and the resulting meltwater, which in turn would lower the sliding friction.

In contrast, the increased roughness of the ski base led to reduced meltwater formation. Transitioning from the finer Linear 1 structure to the rougher Linear 3 consistently decreased meltwater film thickness, despite slightly higher mean pressure for the Linear 3 cases. This effect is attributed to shorter contact durations, which limited the available time for heat accumulation. For example, comparing S5L1F2 and S5L3F2 under identical snow conditions shows a drop in film thickness from 44.8 nm to 29.9 nm. The effect was even more pronounced on ice, where the film thickness dropped from 119 nm in I5L1F2 to 74.6 nm in I5L3F2.

An exception to this general trend was observed in the ice simulations at −15 °C, specifically I15L1F1 and I15L3F1 (Fig. 17). While I15L1F1 exhibited a contact duration nearly twice that of I15L3F1 and a mean pressure almost four times lower, the resulting meltwater film thicknesses were nearly identical. This suggests that under low-temperature conditions, the relationship between pressure, contact duration, and meltwater generation is not straightforward. The limited thermal energy available at colder temperatures may restrict melting regardless of pressure, and longer contact durations may only be effective up to a certain point. These findings highlight the complex interplay between mechanical and thermal variables, particularly when energy input is marginal.

As shown in Section 3.5.2, significantly less meltwater is generated at lower temperatures. The results of this section indicate that a finer ski-base topography promotes greater meltwater formation, likely due to longer contact durations. These findings support the established practice of using a finer ski-base structure for colder conditions, where enhancing meltwater production may help reduce friction.

3.5.4 Effect of Sliding Speed, Multiple Contacts and Refreezing Behaviour

One of the most pronounced effects on meltwater formation was observed when simulating higher sliding speeds and repeated passes. In multiple-pass simulations (MP2, MP5), repeated contact of the same asperities led to cumulative heat build-up, resulting in thicker meltwater films. Increasing the sliding speed from 5 m s^{-1} to 10 m s^{-1} further amplified this effect, especially in the simulated ice cases. As shown in Fig. 18, when the sliding speed was increased to 10 m s^{-1}, the time between the contacts was too short for complete refreezing, allowing the meltwater to persist and accumulate. For example, in run I5L1F2MP2v10, the film thickness reached 313 nm after the second contact.

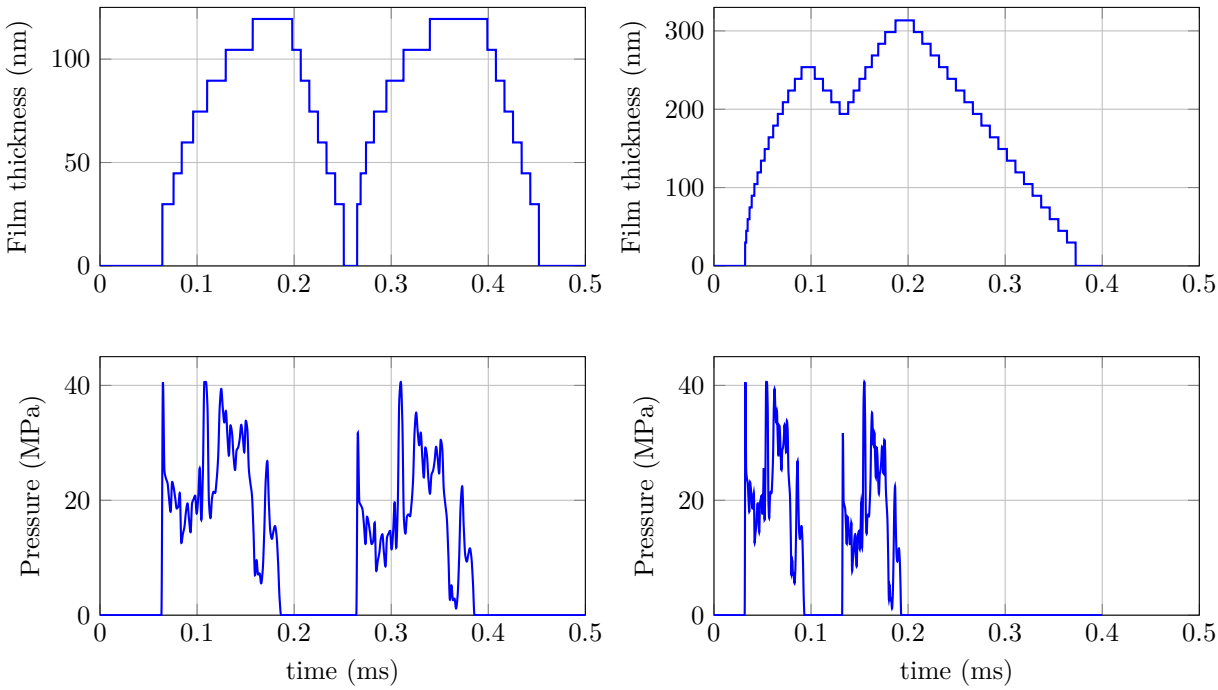

Figure 18: Melt fraction and pressure distribution for I5L1F2MP2 with repeated contacts. (a) Run I5L1F2MP2 at 5 m s^{-1} and (b) Run I5L1F2MP2v10 at 10 m s^{-1}.

The simulations suggest that the snow at the interface rapidly reaches the melting point upon contact. As shown in Fig. 19, the local temperature increases nonlinearly to T_{melt} during loading, then drops when contact is lost, oscillating between the melting point and a subzero minimum. This cyclic thermal behaviour resembles the mechanism proposed by Colbeck [8], who suggested that a point on a slider undergoes repeated heating and cooling. See Appendix B for Colbeck's theorised temperature behaviour.

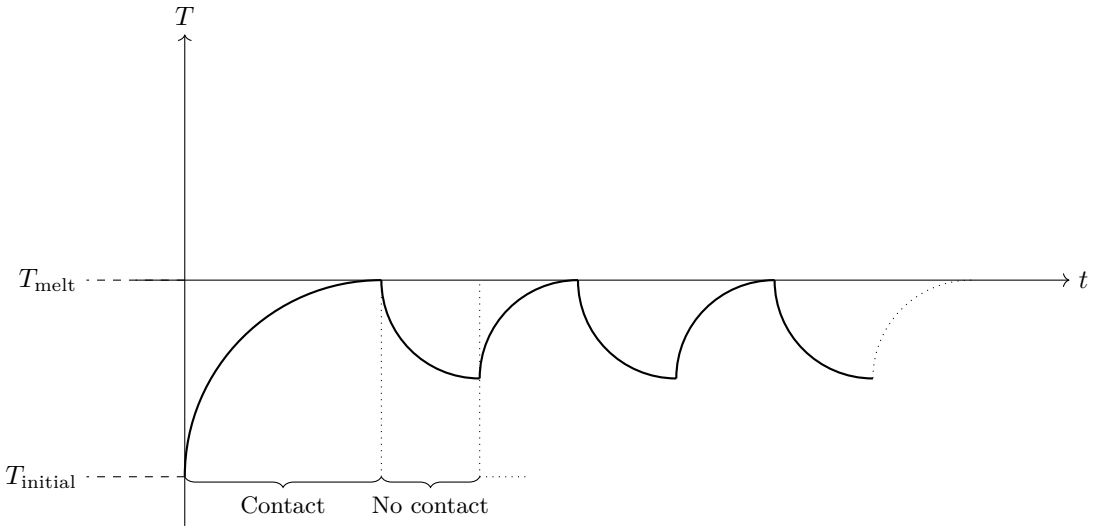

Figure 19: Typical simulated temperature behaviour. The temperature starts at T_{initial} and rapidly increases non-linearly to T_{melt} (initiating phase transition) when contact is made. When contact between the ski and snow asperity is lost, the temperature decreases to a point higher than T_{initial} and the cycle repeats.

This cyclic effect is clearly illustrated in Fig. 20, where the second asperity contact produces a thicker meltwater film than the first. Since the temperature does not decrease all the way to $-15\,^{\circ}\text{C}$ before the second contact, less heat energy is required to increase the temperature to T_{melt}. The reduced thermal requirement allows a larger portion of the available frictional heat to be used for melting, thereby increasing the resulting film thickness.

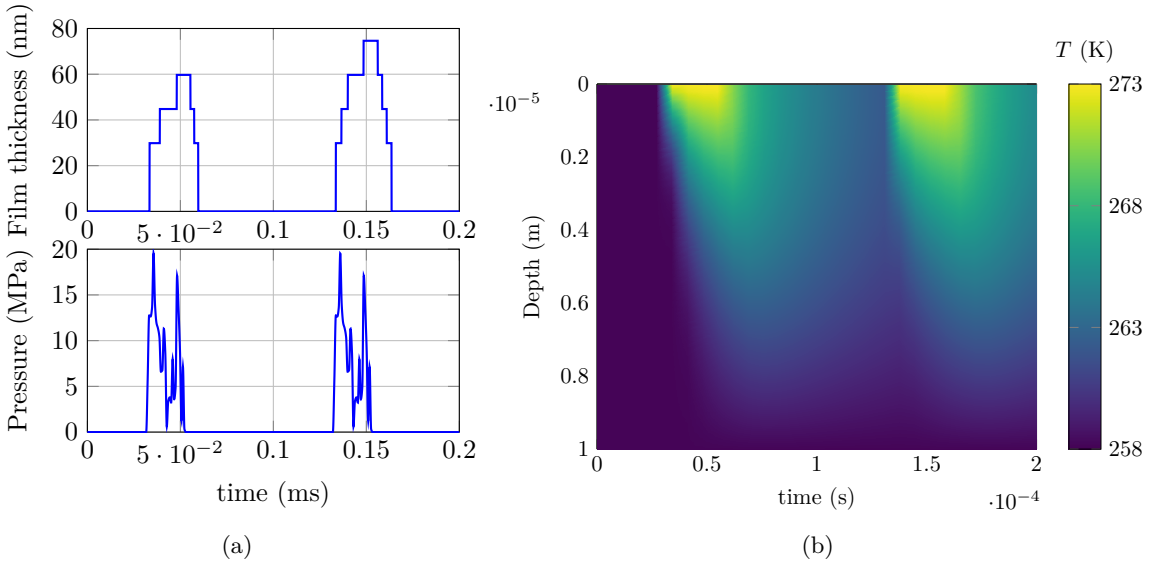

Figure 20: Simulated meltwater formation for I15L1F1MP2v10 (a) Film thickness and pressure distribution showing two sequential asperity contacts. (b) Corresponding temperature evolution within the snow over time and depth, highlighting rapid heating to T_{melt} followed by partial cooling before the second contact.

Refreezing times at $-5\,^{\circ}\mathrm{C}$ were typically on the order of $\mathcal{O}(10\,\mu\mathrm{s})$. Under these conditions, repeated asperity contact may prevent full refreezing between events, allowing meltwater to persist and, thereby, potentially reducing sliding friction. At $-15\,^{\circ}\mathrm{C}$, refreezing occurred too rapidly to enable notable heat accumulation. In some cases, even a small reduction in contact pressure led to immediate refreezing, as seen in Fig. 17a.

3.5.5 Physical Interpretation and Critical Thresholds for Meltwater Generation

The simulations indicate that meltwater generation arises from a balance between contact conditions and the opportunity for refreezing between asperity interactions. The contact pressure and duration stand out as particularly influential for increasing the amount of meltwater. High contact pressures, such as those encountered on ice, and extended contact times, enabled by smoother ski-base structures like Linear 1, both promote greater frictional heating and thus more meltwater. Among the simulated cases, the combination of ice at $-5\,^{\circ}\mathrm{C}$ and the Linear 1 ski-base structure produced the thickest meltwater films, suggesting that this configuration may offer the lowest friction, given that meltwater lubrication is indeed the dominant mechanism. However, excessive meltwater may also increase friction due to capillary effects, in which case a rougher ski-base structure, such as Linear 3, might prove more favourable.

Some meltwater generation appears to occur under most simulated ski–snow conditions, even at $-15\,^{\circ}\mathrm{C}$. However, the rapid refreezing at such cold temperatures limits the persistence of the meltwater film and, consequently, its ability to reduce friction. Several of the simulated cases yielded maximum film thicknesses of 29.9 nm (S5L3F2, S15L1R, S13L3R, and I15L1F1), corresponding to just two spatial steps (Δz thick) in the numerical grid. At these minimal thicknesses, the resolution introduces uncertainty, though a substantially different outcome is not expected even if finer spatial discretisation (Δz) were possible.

Overall, the results suggest that meltwater formation is not driven by a single dominant factor but emerges from the interplay of surface temperature, roughness, contact pressure and duration, and refreezing dynamics. It is this combination that determines the conditions under which frictional melting becomes an effective mechanism for reducing ski–snow friction.

3.6 Model Validation and Sensitivity Analysis

To ensure the robustness and reliability of the simulation results, a validation of the numerical model and a sensitivity analysis were conducted. Model validation compares the numerical predictions with analytical calculations and the sensitivity analysis examines how variations in frictional parameters influence meltwater film formation.

3.6.1 Sensitivity Analysis of Friction Coefficient Parameters

The friction coefficient, as a function of the meltwater thickness (h),

$$\mu(h) = \beta h^3 + \frac{1}{\dfrac{P_{\mathrm{N}} h}{\eta v} + \dfrac{e^{\xi h}}{\epsilon}},$$

(previously presented in Equation (20)), contains the three empirical material parameters ϵ, ξ, and β, which govern the behaviour of the dry, lubricated, and capillary friction components, respectively. These parameters are not directly measurable and are instead estimated to reflect snow and ice conditions, as suggested by [8].

The dry-contact coefficient ϵ can be estimated from experimental data. The exponential parameter ξ controls the rate at which the dry-contact contribution decays with increasing film thickness, while β governs the increase in capillary-induced friction. Since these parameters strongly influence the friction coefficient, a sensitivity analysis was performed using three sets of the parameters ϵ, ξ, β.

The values of the normal pressure (P_{N}), the speed (v), and the viscosity η, which were held constant during all of the simulations, are presented in Table 8. The behaviour of the friction coefficient for meltwater thickness in the range $0 < h \leq 1\,\mu\mathrm{m}$, and $(\epsilon, \xi, \beta) = (0.12, 10^6, 1.5 \cdot 10^{16})$ (red), $(0.2, 10^5, 4.5 \cdot 10^{16})$ (blue), and $(0.3, 10^7, 7.5 \cdot 10^{16})$ (green) is illustrated in Fig. 21.

Table 8: Constant parameter values used in all simulations.

Parameter	Value
P_{N} (MPa)	5
v ($\mathrm{m\,s^{-1}}$)	5
η (Pa · s)	$1.8 \cdot 10^{-3}$

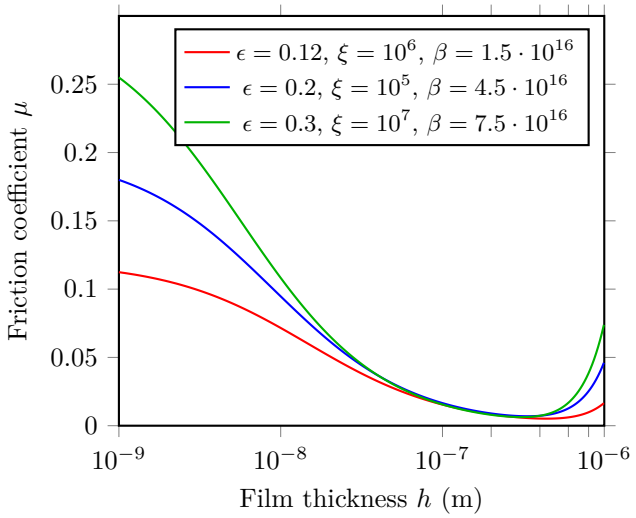

Figure 21: The friction coefficient for meltwater thickness in the range $0 < h \leq 1\,\mu\mathrm{m}$ for parameter sets: (red) $(0.12, 10^6, 1.5{\times}10^{16})$, (blue) $(0.2, 10^5, 4.5{\times}10^{16})$, and (green) $(0.3, 10^7, 7.5{\times}10^{16})$.

The resulting meltwater film thickness after approximately 0.1 ms of contact is reported in Table 9 for each parameter set.

Table 9: Meltwater film thickness after ∼0.1 ms of contact for varying ϵ, ξ, and β values.

Colour	h_{film} (µm)
Red	0.143
Blue	0.157
Green	0.171

From the results presented in Fig. 21, it can be seen that the friction coefficient for h in the range ≈0.1–0.4 µm is virtually the same, but that there are larger discrepancies for smaller and larger values, underscoring that selecting appropriate parameter values is crucial, when using this method to determine the friction coefficient. It is also worth noting is that as pressure increases (with ξ held constant), the lubricated ($\eta v^2/(Ph)$) and dry ($\epsilon/e^{\xi h}$) contributions vanishes and the friction coefficient becomes βh^3, independently on the choice of ξ and ϵ. This asymptotic behaviour highlights that, under high-pressure and thick-film conditions, capillary effects may dominate the frictional response, reinforcing the importance of properly constraining β when modelling such regimes.

3.6.2 Validation Against Analytical Predictions

To evaluate the robustness of the model, the simulation results were compared against the analytical expressions for both contact area and meltwater generation time, derived in Section 2.1, which provide simplified, first-order approximations.

The real contact area was estimated using Equation (5), which assumes idealised plastic contact and neglects the effects of elastic deformation, surface topography, and the pressure distribution. When comparing the calculated contact areas to those produced by the CMS in Table 7, good agreement was observed for snow surfaces, where the contact is largely plastic due to lower hardness. For ice surfaces, however, significant deviations are evident. For instance, in the I5L1F2 case, the simulated contact

area was 0.19 %, while the analytical estimate was only 0.060 %. This discrepancy is attributed to the increasing dominance of elastic contact with surface hardness, reducing the validity of Equation (20). Hence, while the analytical model provides an upper bound for plastic contact, it underperforms under elastic or mixed regimes.

Similarly, the time required to generate a meltwater film of a given thickness was estimated using Equation (20), which incorporates the heat input from friction, heat capacity, and latent heat of fusion under the assumption of uniform film growth under steady conditions. A comparison of simulated and analytically estimated generation times is shown in Fig. 22.

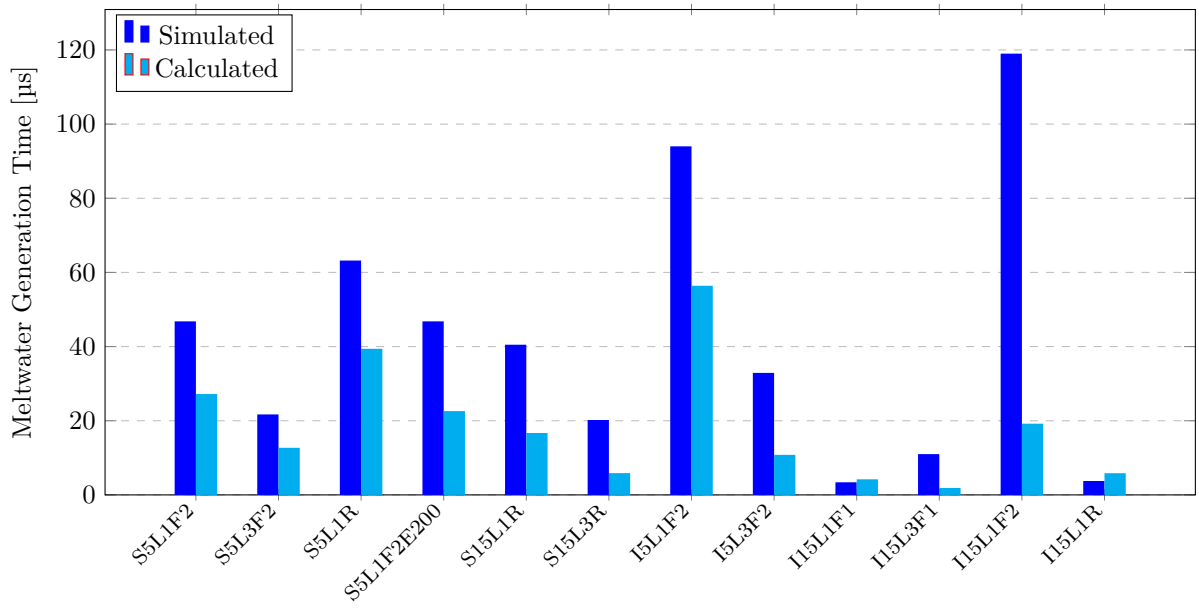

Figure 22: Comparison between simulated meltwater generation times (from FMS) and analytical estimates calculated using Equation (20).

The simulated times refer to the duration required to reach the peak meltwater film thickness in the Frictional Melting Simulations (FMS). In contrast, the calculated times are analytical estimates derived from Equation (20), assuming steady-state growth, constant pressure, and uniform heat input. These estimates serve as simplified benchmarks for evaluating the full simulation results.

Across most simulations, the calculated times showed reasonable agreement with the simulated time (to reach the maximum meltwater thickness simulated from the FMS). For example, in S5L1F2, the simulated time to reach the maximum film thickness was 46.8 µs, while the analytical estimate was 27.2 µs. This underestimation may be due to simplifications in the analytical model, such as the assumption of constant pressure, a constant friction coefficient, and a linear thermal gradient.

These comparisons demonstrate that while analytical models are useful for initial estimates, the accurate prediction of meltwater dynamics, especially in transient, heterogeneous contact scenarios, requires the full numerical approach employed in the CMS-FMS coupling.

4 Concluding Remarks

This section outlines the main results of the simulations and provides a structured analysis of the key trends and behaviours observed. The findings are discussed in relation to the overall objectives and the modelling framework of the study.

4.1 Summary of Objectives and Methods

This work aimed to investigate the thermodynamic processes occurring at the ski–snow interface, particularly focusing on localised frictional heating and its potential to induce melting and form a transient water film. Specifically, the objectives were to:

I. Determine the nature of the ski–snow contact and how it affects meltwater formation.

II. Analyse the influence of ski base textures, varying snow topographies, stiffness, and material properties on melting mechanisms.

III. Identify critical thresholds for meltwater formation under varying conditions.

A numerical simulation framework was developed using a one-dimensional enthalpy-based heat conduction model, capable of resolving phase transitions between ice, water, and refrozen snow. The model encompassed both dry and wet friction regimes, tracking the evolution of meltwater film thickness over time, with contact pressure from a contact mechanics solver serving as input to replicate asperity-scale contact events.

4.2 Key Findings and Contributions

The main findings of the work are:

- **Contact Area Significantly Affects Meltwater Formation:** Simulations show that higher real contact areas on snow correspond to longer contact durations and lower local pressures ($\sim$1.4 MPa), which allow gradual heat build-up and promote meltwater development. In contrast, simulations on ice produce much smaller contact areas but exhibit very high pressures (>30 MPa), resulting in localised, intense heating, and relatively large meltwater films (up to 300 nm).
- **Sliding Speed and Repeated Contact Increase Melting:** Simulations with increased velocity ($10\,\mathrm{m\,s^{-1}}$) and repeated passes (MP2, MP5) on ice surfaces resulted in significantly thicker meltwater films. This suggests that heat accumulation across successive asperity contacts is a dominant mechanism in real skiing.
- **Surface Roughness Plays Dual Roles:** Rougher snow surfaces increase contact durations due to more pronounced plastic deformation, enhancing meltwater generation. In contrast, rougher ski bases consistently reduce contact duration and area, limiting meltwater generation.
- **Temperature Effects Are Strongly Nonlinear:** Lower temperatures significantly reduce the generation of meltwater due to both the reduction in snow/ice temperature and the increase in the hardness of the material, which reduces the contact durations. However, melting is still observed even at colder temperatures ($-15\,^\circ$C).
- **Analytical Time Predictions Deviate from Simulations:** Equation (20) often underestimates the time needed to form the observed meltwater thicknesses, particularly in contact cases of high pressure and short duration. This highlights the importance of transient modelling over static approximations in capturing frictional melting dynamics.

In summary, this work demonstrates that the generation of frictional meltwater is governed by an interplay between pressure, time, roughness, and temperature. The proposed modelling framework captures these dependencies and offers a tool for future exploration of ski–snow dynamics under racing conditions.

4.3 Alignment with Objectives

The results of this work closely align with the stated objectives. The simulations effectively revealed how ski–snow contact characteristics influence meltwater formation, fulfilling Objective 1. By systematically varying base textures, snow topographies, and material properties, the study addressed Objective 2, demonstrating how surface roughness, temperature, and mechanical properties shape the melting response.

Objective 3 was met through the identification of critical combinations of pressure, duration, and speed that enable meltwater formation, even under cold and high-pressure conditions. The developed simulation framework successfully captured transient thermal processes and phase transitions, providing a mechanistic understanding of frictional melting at the interface.

4.4 Delimitations

The model presented in this work contains several simplifications. Most notably, the domain of the FMS was one-dimensional, ignoring lateral heat conduction. The melting point was assumed to be constant, without accounting for pressure-dependent lowering of the melting temperature, an effect that may be relevant at high pressures, which would increase meltwater generation. In addition, while the pressure input was designed to mimic realistic contact sequences, it was synthetically generated rather than derived from experimental data.

Furthermore, the model does not include coupling to the Reynolds equation, which would be necessary to simulate the hydrodynamic pressure in the meltwater film and its feedback on contact mechanics. Such a coupling would provide a more complete picture of the lubrication behaviour.

4.5 Suggestions for Future Work

Future research could build on this foundation in several ways. A natural next step would be to implement a three-dimensional version of the model to capture lateral heat conduction and nonuniform pressure distributions. Coupling the thermal model with a complete Reynolds equation solver would enable simulation of fluid behaviour and its effect on load-carrying capacity, potentially allowing the model to predict transition thresholds from boundary to hydrodynamic lubrication.

Experimental validation would also be valuable. For example, pressure-sensitive films or infrared thermography could be used to measure real-time temperature and contact pressure distributions during ski gliding.

Lastly, integrating this type of microscale modelling into macroscale simulations of entire skis using a statistical ensemble of asperity contacts could bridge the gap between fundamental thermal processes and observed ski performance on snow.

References

[1] F. P. Bowden, T. P. Hughes, and C. H. Desch. "The mechanism of sliding on ice and snow". In: *Proceedings of the Royal Society of London. Series A. Mathematical and Physical Sciences* 172.949 (1939), pp. 280–298. DOI: 10.1098/rspa.1939.0104.

[2] W. Ambach and B. Mayr. "Ski gliding and water film". In: *Cold Regions Science and Technology* 5.1 (1981), pp. 59–65. DOI: 10.1016/0165-232X(81)90040-9.

[3] M. Hasler, W. Jud, and W. Nachbauer. "Snow Temperature Behind Sliding Skis as an Indicator for Frictional Meltwater". In: *Frontiers in Mechanical Engineering* 7 (2021), p. 738266. DOI: 10.3389/fmech.2021.738266.

[4] M. Hasler, K. Schindelwig, B. Mayr, C. Knoflach, S. Rohm, J. van Putten, and W. Nachbauer. "A Novel Ski–Snow Tribometer and its Precision". In: *Tribology Letters* 64.1 (2016), p. 19. DOI: 10.1007/s11249-016-0719-2.

[5] M. Hasler, K. Schindelwig, and J. Van Putten. "Temperature Below a Gliding Cross-Country Ski". In: *Procedia Engineering* 72 (2014), pp. 380–385.

[6] S. Auganæs, A. Buene, and A. Klein-Paste. "The effect of load and binding position on the friction of cross-country skis". In: *Cold Regions Science and Technology* 212 (May 2023), p. 103884. DOI: 10.1016/j.coldregions.2023.103884.

[7] K. Kalliorinne, B. N. J. Persson, J. Sandberg, G. Hindér, R. Larsson, H.-C. Holmberg, and A. Almqvist. "Characterisation of the Contact Between Cross-Country Skis and Snow: A Micro-Scale Study Considering the Ski-Base Texture". In: *Lubricants* 11.5 (2023). DOI: 10.3390/lubricants11050225.

[8] S. C. Colbeck. *A review of the processes that control snow friction.* 1992.

[9] S. A. Siddiqui, M. Hasler, M. Mössner, J. van Putten, K. Schindelwig, and W. Nachbauer. "Detection of Frictional Meltwater on Snow Surface Using a Humidity Indicator". In: *Current Issues in Sport Science (CISS)* 9.4 (2024). DOI: 10.36950/2024.4ciss010.

[10] L. Bäurle, T. Kaempfer, D. Szabó, and N. Spencer. "Sliding friction of polyethylene on snow and ice: Contact area and modeling". In: *Cold Regions Science and Technology* 47.3 (2007), pp. 276–289. DOI: 10.1016/j.coldregions.2006.10.005. URL: https://www.sciencedirect.com/science/article/pii/S0165232X06001625.

[11] J. H. Lever, S. Taylor, A. J. Song, Z. R. Courville, R. Lieblappen, and J. C. Weale. "The mechanics of snow friction as revealed by micro-scale interface observations". In: *Journal of Glaciology* 64 (2017), pp. 27–36.

[12] K. Kalliorinne, G. Hindér, J. Sandberg, H.-C. Holmberg, R. Larsson, and A. Almqvist. "On the Multi-Scale Nature of Ski–Snow Friction in Cold Conditions". In: *Friction* (Feb. 2025). DOI: 10.26599/FRICT.2025.9441069.

[13] M. Takeda, K. Nikki, T. Nishizuka, and O. Abe. "Friction of the short model ski at low velocity". In: *Journal of Physics: Conference Series* 258 (Dec. 2010), p. 012007. DOI: 10.1088/1742-6596/258/1/012007.

[14] A. Atila, S. V. Sukhomlinov, and M. H. Müser. "Cold self-lubrication of sliding ice". In: *arXiv* (2024). arXiv: 2402.10843. URL: https://arxiv.org/abs/2402.10843.

[15] B. Weber, Y. Nagata, S. Ketzetzi, F. Tang, W. J. Smit, H. J. Bakker, E. H. G. Backus, M. Bonn, and D. Bonn. "Molecular insight into the slipperiness of ice". In: *Journal of Physical Chemistry Letters* 9 (2018), pp. 2838–2842.

[16] A.-M. Kietzig, S. Hatzikiriakos, and P. Englezos. "Ice friction: The effects of surface roughness, structure, and hydrophobicity". In: *Journal of Applied Physics* 106 (Aug. 2009), pp. 024303–024303. DOI: 10.1063/1.3173346.

[17] S. Colbeck. "The Kinetic Friction of Snow". In: *Journal of Glaciology* 34.116 (1988), pp. 78–86. DOI: 10.3189/S0022143000009096.

[18] S. Ducret, H. Zahouani, A. Midol, P. Lanteri, and T. Mathia. "Friction and abrasive wear of UHWMPE sliding on ice". In: *Wear* 258 (Jan. 2005), pp. 26–31. DOI: 10.1016/j.wear.2004.09.026.

[19] D. Evans, J. Nye, and K. Cheeseman. "The Kinetic Friction of Ice". In: *Proceedings of The Royal Society A: Mathematical, Physical and Engineering Sciences* 347 (Jan. 1976), pp. 493–512. DOI: 10.1098/rspa.1976.0013.

[20] B. Persson. *Sliding Friction: Physical Principles and Applications*. NanoScience and Technology. Springer Berlin Heidelberg, 1998. URL: https://books.google.se/books?id=biRRAAAAMAAJ.

[21] M. Akkök, C. Ettles, and S. Calabrese. "Parameters Affecting the Kinetic Friction of Ice". In: *Journal of Tribology-transactions of The Asme - J TRIBOL-TRANS ASME* 109 (July 1987). DOI: 10.1115/1.3261503.

[22] A. Lehtovaara. "Influence of vibration on the kinetic friction between plastics and ice". In: *Wear* 115.1 (1987), pp. 131–138. DOI: 10.1016/0043-1648(87)90204-3.

[23] J. Lever, E. Asenath-Smith, S. Taylor, and A. Lines. "Assessing the Mechanisms Thought to Govern Ice and Snow Friction and Their Interplay With Substrate Brittle Behavior". In: *Frontiers in Mechanical Engineering* 7 (June 2021). DOI: 10.3389/fmech.2021.690425.

[24] S. Jacobson and S. Hogmark. *Tribologi : friktion, smörjning och nötning*. 1. utg. Stockholm: Liber utbildning, 1996.

[25] F. Incropera, D. DeWitt, T. Bergman, and A. Lavine. *Fundamentals of Heat and Mass Transfer*. Jan. 2007.

[26] C. Swaminathan and V. Voller. "On the enthalpy method". English (US). In: *International Journal of Numerical Methods for Heat & Fluid Flow* 3.3 (Mar. 1993), pp. 233–244. DOI: 10.1108/eb017528.

[27] E. Gadelmawla, M. Koura, T. Maksoud, I. Elewa, and H. Soliman. "Roughness parameters". In: *Journal of Materials Processing Technology* 123.1 (2002), pp. 133–145. DOI: 10.1016/S0924-0136(02)00060-2.

[28] Evident. *Surface Roughness Measurement—Parameters*. 2025. URL: https://evidentscientific.com/en/applications/metrology/surface-roughness-measurement-portal/parameters#007.

[29] M. Hasler, M. Mössner, W. Jud, K. Schindelwig, M. Gufler, J. van Putten, S. Rohm, and W. Nachbauer. "Wear of snow due to sliding friction". In: *Wear* 510-511 (2022), p. 204499. DOI: 10.1016/j.wear.2022.204499. URL: https://www.sciencedirect.com/science/article/pii/S0043164822002563.

[30] A. Almqvist. *Fractal Surface Generator*. MATLAB Central File Exchange. Retrieved April 20, 2025. 2025. URL: https://www.mathworks.com/matlabcentral/fileexchange/129469-fractal-surface-generator.

[31] Y. Takeuchi, Y. Nohguchi, K. Kawashima, and K. Izumi. "Measurement of snow-hardness distribution". In: *Annals of Glaciology* 26 (1998), pp. 27–30. DOI: 10.3189/1998AoG26-1-27-30.

[32] K. Tusima. "The temperature dependence of hardness of snow". In: 2007. URL: https://api.semanticscholar.org/CorpusID:199563754.

[33] L. Makkonen and M. Tikanmäki. "Modeling the friction of ice". In: *Cold Regions Science and Technology* 102 (2014), pp. 84–93. DOI: 10.1016/j.coldregions.2014.03.002. URL: https://www.sciencedirect.com/science/article/pii/S0165232X14000561.

[34] C. Nayak, P. Kushram, M. A. A. Zaidi, I. Singh, J. Sen, and K. Balani. "Multi-length scale strengthening and cytocompatibility of ultra high molecular weight polyethylene bio-composites by functionalized carbon nanotube and hydroxyapatite reinforcement". In: *Journal of the Mechanical Behavior of Biomedical Materials* 140 (2023), p. 105694. DOI: 10.1016/j.jmbbm.2023.105694.

[35] H. Han, M. Yang, X. Liu, Y. Li, G. Gao, and E. Wang. "Study on the Constitutive Equation and Mechanical Properties of Natural Snow under Step Loading". In: *Water* 15.18 (2023). DOI: 10.3390/w15183271. URL: https://www.mdpi.com/2073-4441/15/18/3271.

[36] N. Lintzen and T. Edeskär. "Uniaxial Strength and Deformation Properties of Machine-Made Snow". In: *Journal of Cold Regions Engineering* 29 (Sept. 2014), p. 04014020. DOI: 10.1061/(ASCE)CR.1943-5495.0000090.

[37] J. Petrovic. "Review Mechanical properties of ice and snow". In: *Journal of Materials Science* 38 (Jan. 2003), pp. 1–6. DOI: 10.1023/A:1021134128038.

[38] Y. C. Yen. *Review of thermal properties of snow, ice and sea ice*. Tech. rep. CRREL Report 81-10. Hanover, New Hampshire: U.S. Army Corps of Engineers, Cold Regions Research and Engineering Laboratory, 1981.

[39] M. Sturm, J. Holmgren, M. König, and K. Morris. "The thermal conductivity of seasonal snow". In: *Journal of Glaciology* 43.143 (1997), pp. 26–41. DOI: 10.3189/S0022143000002781.

[40] A. Almqvist, F. Sahlin, R. Larsson, and S. Glavatskih. “On the Dry Elasto-Plastic Contact of Nominally Flat Surfaces”. In: *Tribology International* 40.4 (2007), pp. 574–579. DOI: 10.1016/j.triboint.2006.06.006.

[41] F. Sahlin, R. Larsson, A. Almqvist, P. M. Lugt, and P. Marklund. “A Mixed Lubrication Model Incorporating Measured Surface Topography. Part 1: Theory of Flow Factors”. In: *Proceedings of the Institution of Mechanical Engineers, Part J: Journal of Engineering Tribology* 224.3 (2010), pp. 335–351. DOI: 10.1243/13506501JET691.

[42] A. Almqvist, C. Campana, N. Prodanov, and B. N. J. Persson. “Interfacial Separation between Elastic Solids with Randomly Rough Surfaces: Comparison between Theory and Numerical Techniques”. In: *Journal of the Mechanics and Physics of Solids* 59.11 (2011), pp. 2355–2369. DOI: 10.1016/j.jmps.2011.08.004.

[43] A. Tiwari, A. Almqvist, and B. N. J. Persson. “Plastic Deformation of Rough Metallic Surfaces”. In: *Tribology Letters* 68.4 (2020), p. 129. DOI: 10.1007/s11249-020-01368-9.

[44] F. Pérez-Ràfols and A. Almqvist. “On the Stiffness of Surfaces with Non-Gaussian Height Distribution”. In: *Scientific Reports* 11.1 (2021), p. 1863. DOI: 10.1038/s41598-021-81259-8.

[45] K. Kalliorinne, R. Larsson, F. Pérez-Ràfols, M. Liwicki, and A. Almqvist. “Artificial Neural Network Architecture for Prediction of Contact Mechanical Response”. In: *Frontiers in Mechanical Engineering* 6 (2021), p. 579825. DOI: 10.3389/fmech.2020.579825.

[46] K. Kalliorinne, J. Sandberg, G. Hindér, R. Larsson, H.-C. Holmberg, and A. Almqvist. *Snow contact characterisation of cross-country skis: A macro-scale study of the apparent contact*. Aug. 2022. DOI: 10.20944/preprints202208.0512.v1.

[47] R. Eriksson and W. Nupen. “FRICTION OF RUNNERS ON SNOW AND ICE”. In: (1955).

A Snow and Ice Surfaces

Surface Rough

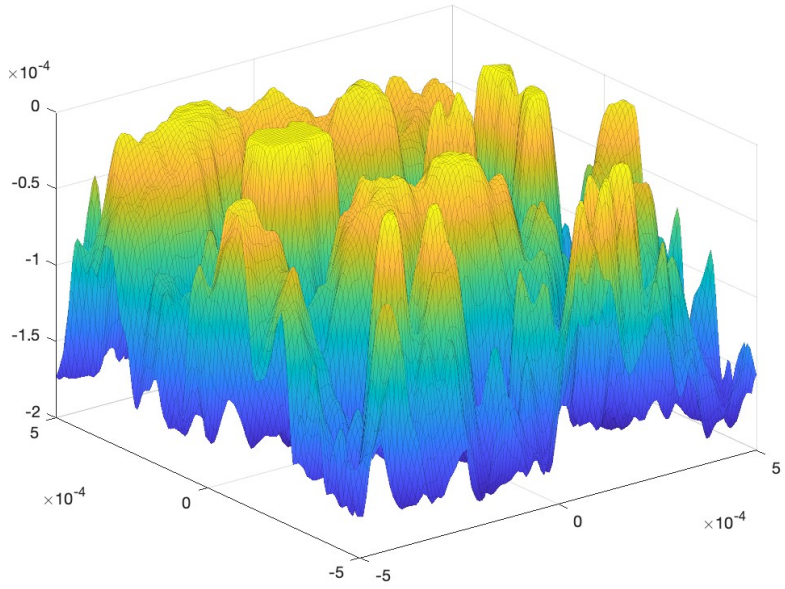

Figure 23: Surface Rough

Ice Surface

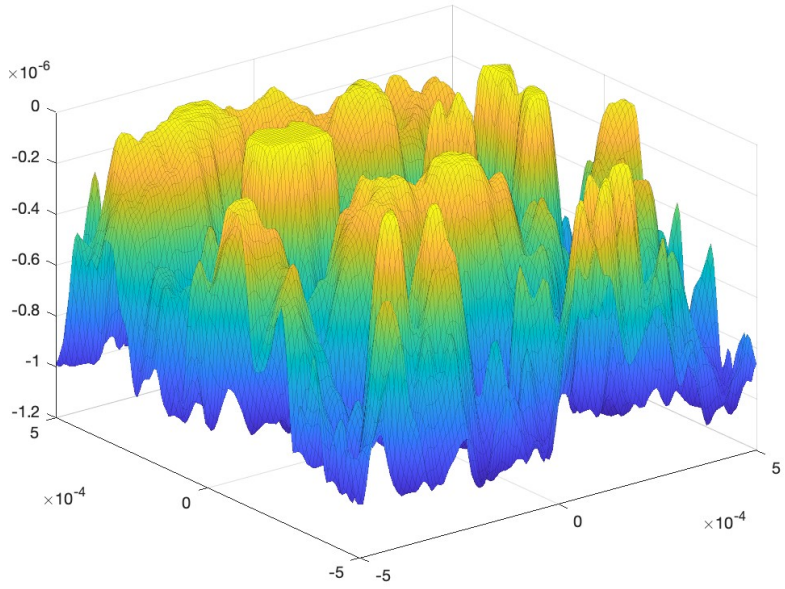

Figure 24: Ice Surface

B Theorised Temperature Behaviour

This section presents the temperature of a point on a slider as it passes over snow, theorised by Colbeck [8].

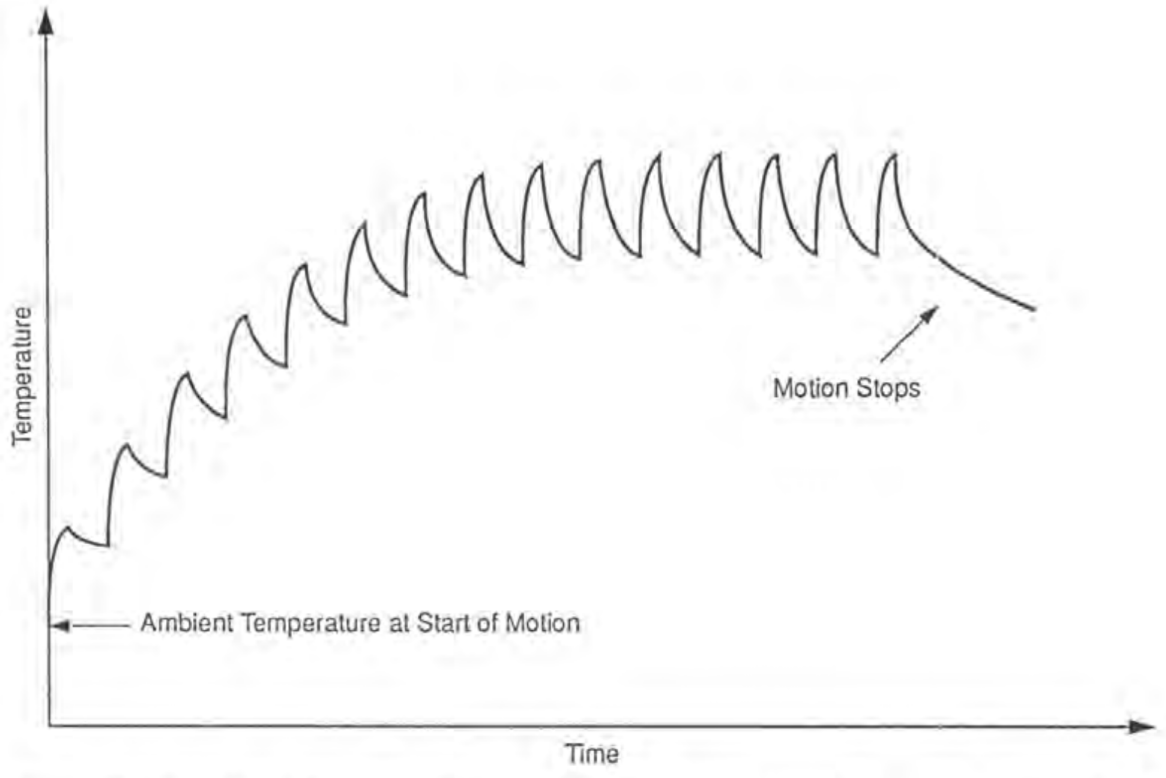

Figure 25: Figure adapted from Colbeck [8].